

REPORT DOCUMENTATION PAGE		READ INSTRUCTIONS BEFORE COMPLETING FORM
1. REPORT NUMBER NRL Report 7887	2. GOVT ACCESSION NO.	3. RECIPIENT'S CATALOG NUMBER
4. TITLE (and Subtitle) AN EXPERIMENTAL DESCRIPTION OF A FREE-FLOODED FINITE-LENGTH RADIATING MAGNETOSTRICTIVE RING TRANSDUCER	5. TYPE OF REPORT & PERIOD COVERED Interim report on a continuing NRL Problem	
	6. PERFORMING ORG. REPORT NUMBER	
7. AUTHOR(s) Joel A. Sinsky	8. CONTRACT OR GRANT NUMBER(s)	
9. PERFORMING ORGANIZATION NAME AND ADDRESS Naval Research Laboratory Washington, D.C. 20375	10. PROGRAM ELEMENT, PROJECT, TASK AREA & WORK UNIT NUMBERS Project NRL Problem S02-19 XF 11-121-100 Task 1-01-01	
11. CONTROLLING OFFICE NAME AND ADDRESS Naval Electronics Systems Command Code 320 Washington, D.C. 20360	12. REPORT DATE June 4, 1975	
	13. NUMBER OF PAGES	
14. MONITORING AGENCY NAME & ADDRESS (if different from Controlling Office)	15. SECURITY CLASS. (of this report) UNCLASSIFIED	
	15a. DECLASSIFICATION/DOWNGRADING SCHEDULE	
16. DISTRIBUTION STATEMENT (of this Report) Approved for public release: distribution unlimited.		
17. DISTRIBUTION STATEMENT (of the abstract entered in Block 20, if different from Report)		
18. SUPPLEMENTARY NOTES		
19. KEY WORDS (Continue on reverse side if necessary and identify by block number) Magnetostriuctive materials Magnetostriiction transducers Free-flooded rings Underwater sound sources Acoustic measurements		
20. ABSTRACT (Continue on reverse side if necessary and identify by block number) The electrical input impedances and acoustic radiation characteristics of magnetostriuctive scroll-wound ring transducers were carefully measured and documented to provide experimental data for comparison with theoretical ring-transducer models. Conventional-nickel and cube-textured-nickel rings with equivalent diameter and thickness but with varying lengths were used in the experiment. The data were compared to the theoretical model, NRL EIGSHIP, a computer program of a mathematical analysis of the electroacoustic performance of a single finite-length magnetostriuctive circular cylinder submerged in an unbounded medium and radiating sound. The		

20. Continued

experiment is described, the data are tabulated and plotted, possible sources of error are suggested, and a comparison is made with theory.

CONTENTS

Principal Symbols Used	iv
INTRODUCTION	1
APPARATUS	1
EXPERIMENTAL DATA	3
ANALYSIS	11
CALCULATIONS	18
CONCLUSIONS	26
ACKNOWLEDGMENTS	27
REFERENCES	27
APPENDIX A — Theoretical Predictions From the Computer Program NRL EIGSHIP and Comparison With Experiment	29
APPENDIX B — A 1.9-Inch-High Ring	38
APPENDIX C — A 3.6-Inch-High Ring (Cylinder)	45

PRINCIPAL SYMBOLS USED

A_0	cross-sectional area of the ring core
a	mean radius of the ring core
M	mass of the ring core
N	number of toroidal windings around the ring core
A_{coil}	average cross-sectional area enclosed in the toroidal windings
f	frequency of excitation
Z_T	total electrical input impedance
r_w	dc resistance of the toroidal windings
X_c	core reactance
X_b	core reactance at the radial resonance frequency
χ	the eddy-current vector
ζ, η	loss angles
R_m	total mechanical resistance
X_m	mechanical reactance
R_{mp}	mechanical resistance corresponding to other than eddy-current losses
D_z	diameter of the motional impedance circle
Q_z	quality factor
g_{33}	piezomagnetic constant relating circumferential strain and circumferential magnetic induction
S_{33}^B	elastic compliance at constant magnetic induction
μ_{33}^T	reversible permeability at constant stress
μ_{33}^S	reversible permeability at constant strain
k	effective electromechanical coupling coefficient
k_{33}	material electromechanical coupling coefficient

AN EXPERIMENTAL DESCRIPTION OF A FREE-FLOODED FINITE-LENGTH RADIATING MAGNETOSTRICTIVE RING TRANSDUCER

INTRODUCTION

The electrical input impedances and acoustic radiation characteristics of magnetostrictive scroll-wound ring transducers were carefully measured and documented to provide experimental data for comparison with theoretical ring-transducer models. The ring transducers used in the experiment described in the body of this report and in Appendix A were a ring fabricated from conventional Nickel 200 at the Naval Underwater Systems Center, New London, Connecticut, and a ring of nearly identical dimensions fabricated from cube-textured nickel at the International Nickel Company, Suffern, New York [1]. Both transducers were separately excited in air and in water under nearly identical physical conditions and induction fields, and their electrical input impedances were measured on a Pulse Vector Immittance Meter. Far-field polar plots and transmitting-current responses were also recorded of the in-water performance of the transducers. Elastic, magnetostrictive, and acoustic properties of the transducers were derived from the electrical-impedance and acoustic-radiation measurements. In addition results of measurements are given on a longer cube-textured-nickel ring in Appendix B and on a cube-textured-nickel cylinder in Appendix C. The transducer engineer can use a computer program, with a confidence level defined by agreement between theory and experiment, to design a magnetostrictive ring transducer in the same regime of relative dimensions as the test rings. NRL EIGSHIP is a computer program of a mathematical analysis of the electroacoustic performance of a single finite-length magnetostrictive circular cylinder submerged in an unbounded medium and radiating sound [2]. Agreement between experiment and the comprehensive program NRL EIGSHIP was quite good for the in-air measurements and satisfactory for the in-water measurements.

APPARATUS

The ring transducers used were wire-wound magnetostrictive cores (Fig. 1). The core materials were conventional Nickel 200, which is also called "A" Nickel, and the INCO cube-textured nickel (CTN). The ring cores were scroll wound, which means that they were made by winding a metal strip about a mandrel and using a bonding agent to consolidate the windings permanently. The Nickel 200 strip was 0.007 inch thick, and the CTN strip was 0.008 inch thick. Table 1 gives the average dimensions of the finished cores of the two rings with nearly identical dimensions. The accuracy of the measurements was ± 0.0001 m and ± 0.0001 kg.

Each of the cores was separately mounted as shown in Fig. 1. The mounting structure was designed to hold a core in a fixed position in the windings while providing the least possible clamping of the core and to be acoustically invisible in the excitation

Note: Manuscript submitted March 20, 1975.

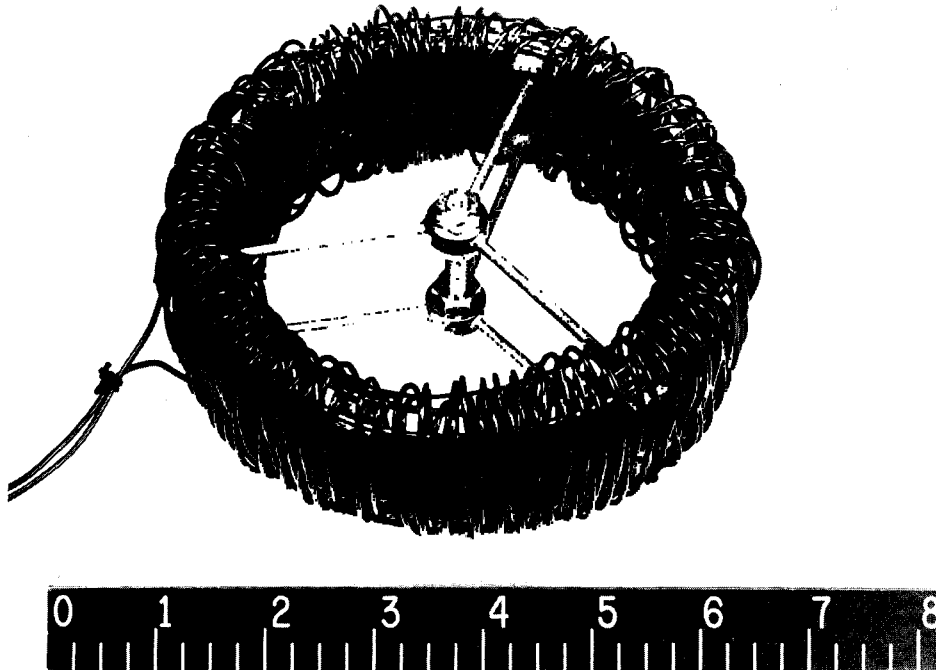


Fig. 1 — A ring transducer

Table 1
Average Dimensions and Masses of the Finished Cores

Ring	Outside Diameter (m)	Inside Diameter (m)	Height (m)	Mean Radius (m)	Mass (kg)
CTN	0.1382	0.1249	0.02029	0.06578	0.4591
Nickel 200	0.1379	0.1250	0.01942	0.06573	0.4338

frequency range of interest. The 144 toroidal turns of No. 18 Teflon-insulated wire were supported by four copper hoops above and below the ring core, and the hoops in turn were supported by two sets of three spokes emanating from hubs at the geometric center of the ring transducer. The hubs were held apart and the entire structure was kept rigid by a threaded 1/4-inch bolt and four nuts. The motion of the core was isolated from the supporting structure by pads of rho-C rubber. This mounting structure contains numerous modifications of previous structures which used bulkier hardware and solid Bakelite winding supports that pressed tightly against the ring core. The toroidal windings were kept uniformly spaced around the ring by O-ring stock which was woven circumferentially through the windings. The average cross-sectional areas enclosed in the windings were:

$$A_{\text{coil}} = 1.219 \times 10^{-3} \text{ m}^2 \text{ for the CTN ring,}$$

$$A_{\text{coil}} = 1.070 \times 10^{-3} \text{ m}^2 \text{ for the Nickel 200 ring.}$$

For the air and water impedance measurements the rings were hung with the center bolt vertical by single pieces of stiff single-conductor wire attached to the center bolt. For the far-field polar plots and transmitting current responses the rings were supported with the center bolt horizontal from a vertical shaft. The shaft was rotatable and rigidly suspended from a Scientific Atlanta Positioner Unit mounted at the top of the NRL Acoustic Research Tank, in which all of the in-water measurements were done.

Each ring was simultaneously excited by a dc magnetizing current and an ac driving current. The blocking circuit which isolated the ac current from the dc current source is diagrammed in Fig. 2.

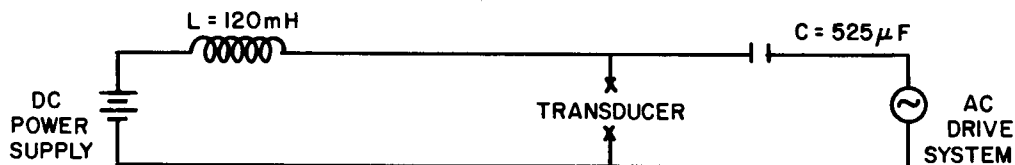


Fig. 2 — Blocking circuit to isolate the current sources

The block circuit diagrams of the transducer driving system and the receiving system are shown in Figs. 3a and 3b [3]. The in-air impedance measurements were done CW; therefore the pulse timing generator and transmitter gate in the driving system were switched off. For the in-water measurements the pulse-modulated driving signal and gated measuring system allowed determination of free-field steady-state data in the confined space of the calibration tank. The hydrophone used in the experiment was a Navy Underwater Sound Reference Laboratory Model F36 whose sensitivity was -202.4 dB re $1 V/\mu Pa$ [4]. A Scientific Atlanta Pulse Vector Immittance Meter measured the input electrical resistance and reactance of the transducer and blocking circuit. The dc magnetizing current was 4.0 amperes for the CTN ring and 3.8 amperes for the Nickel 200 ring. These current levels corresponded to magnetizing induction-field levels of 3.8 and 3.9 kilogauss respectively in the two rings. The ac drive current level was held constant at 15 milliamperes rms by a current normalizer for all of the electrical-input-impedance measurements and held constant at 100 milliamperes for the transmitting responses and polar plots. The Pulse Vector Immittance Meter was calibrated each day of the experiment with a standard 500-microhenry choke at 10 kilohertz. The receiving system was calibrated each day by replacing the hydrophone by an oscillator and a voltmeter.

EXPERIMENTAL DATA

An experimental impedance run on a ring transducer corresponded to input-electrical-impedance measurements at various frequencies of ac excitation. For each run the core impedance was measured in air every 500 Hz in the frequency range 500 to 50,000 Hz. Approximately 60 values of impedance were then measured at or near radial resonance in air and in water to define the impedance circle resulting from a plot of electrical input reactance versus electrical input resistance. During each run a plot of input reactance versus input resistance was drawn by a chart recorder as the numerical values of these quantities were being recorded from the Pulse Vector Immittance Meter.

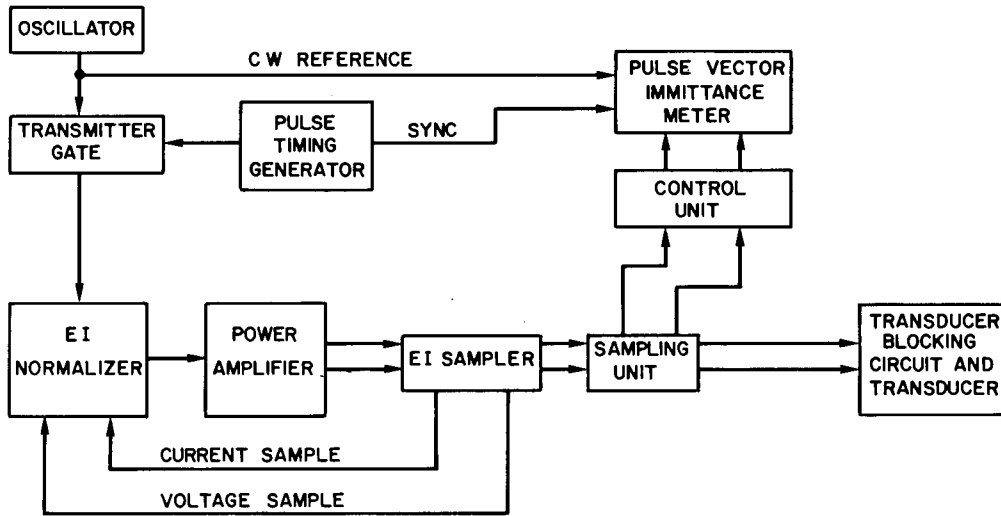


Fig. 3a — Transducer driving system

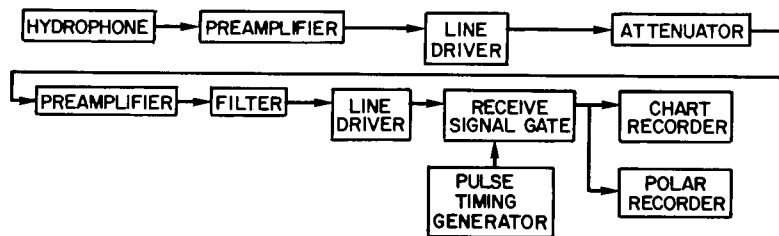


Fig. 3b — Receiving system

The simultaneous plot, although not used for data, was useful in visually indicating the frequencies at which impedance data should be recorded. The data were corrected for the contribution to the total input electrical impedance from the blocking circuit. The resulting numerical data are given for the CTN-ring core impedance in Table 2a and for the Nickel-200-ring core impedance in Table 2b. Figures 4a and 4b are plots of core reactance vs frequency for the CTN and Nickel 200 rings. In-air impedance values corresponding to frequencies near resonance are given for the CTN ring in Table 3a and for the Nickel 200 ring in Table 3b. Figure 5a shows the in-air impedance circle of the CTN ring, and Fig. 5b shows the in-air impedance circle of the Nickel 200 ring, which are plots of the data in Tables 3a and 3b respectively. Each point on the plots corresponds to a specific frequency of ring excitation, and the total electrical input impedance at the frequency is the length of a vector drawn from the origin of coordinates to the point. In-water resonance values are given in Table 4a for the CTN ring and in Table 4b for the Nickel 200 ring. Figures 6a and 6b show the in-water impedance circles of the CTN ring and the Nickel 200 ring and are plots of the data in Tables 4a and 4b respectively. At frequencies well below and well above the air and water resonance frequencies, the core impedances of the rings in water were the same as the core impedances of the rings in air.

Table 2a
 Core Impedance of the CTN Ring in Air
 (system error = ± 1 ohm; reading error = ± 0.1 ohm)

Frequency (Hz)	Resistance (ohms)	Reactance (ohms)	Frequency (Hz)	Resistance (ohms)	Reactance (ohms)
500	0.8	0.7	25,500	5.4	34.6
1,000	0.8	1.4	26,000	5.6	35.2
1,500	0.7	2.2	26,500	5.8	36.0
2,000	0.7	2.9	27,000	6.0	36.5
2,500	0.7	3.6	27,500	6.1	37.2
3,000	0.7	4.4	28,000	6.2	37.8
3,500	0.8	5.3	28,500	6.5	38.3
4,000	0.8	6.1	29,000	6.7	39.0
4,500	0.8	6.8	29,500	7.2	39.3
5,000	0.8	7.5	30,000	7.1	40.1
5,500	0.9	8.4	30,500	7.3	40.9
6,000	1.0	9.3	31,000	7.5	41.5
6,500	1.1	10.1	31,500	7.7	42.1
7,000	1.2	11.0	32,000	8.0	42.7
7,500	1.3	12.2	32,500	8.2	43.4
8,000	1.5	13.6	33,000	8.5	43.9
8,500	2.0	16.0	33,500	8.7	44.6
9,000	5.5	26.2	34,000	8.9	45.2
9,500	1.4	2.0	34,500	9.1	45.8
10,000	1.0	9.8	35,000	9.4	46.4
10,500	1.2	12.1	35,500	9.6	47.0
11,000	1.3	13.5	36,000	9.9	47.6
11,500	1.6	14.6	36,500	10.1	48.2
12,000	1.6	15.6	37,000	10.4	48.8
12,500	1.7	16.5	37,500	10.6	49.4
13,000	1.9	17.3	38,000	10.9	50.0
13,500	2.0	18.0	38,500	11.2	50.6
14,000	2.0	18.8	39,000	11.3	51.2
14,500	2.2	19.6	39,500	11.5	51.7
15,000	2.3	20.8	40,000	11.9	52.3
15,500	2.4	21.1	40,500	12.1	53.0
16,000	2.6	21.8	41,000	12.4	53.6
16,500	2.6	22.5	41,500	12.7	54.1
17,000	2.8	23.2	42,000	13.0	54.7
17,500	2.9	23.9	42,500	13.3	55.2
18,000	3.1	24.5	43,000	13.5	55.8
18,500	3.2	25.2	43,500	13.8	56.5
19,000	3.3	26.0	44,000	14.1	56.9
19,500	3.4	26.7	44,500	14.3	57.5
20,000	3.6	27.2	45,000	14.7	58.1
20,500	3.8	28.0	45,500	14.9	58.6
21,000	3.9	28.5	46,000	15.3	59.1
21,500	4.0	29.3	46,500	15.5	59.7
22,000	4.2	29.9	47,000	15.9	60.4
22,500	4.4	30.6	47,500	16.2	60.7
23,000	4.6	31.3	48,000	16.5	61.4
23,500	4.7	31.9	48,500	16.8	61.9
24,000	4.8	32.6	49,000	17.1	62.5
24,500	5.0	33.3	49,500	17.4	63.0
25,000	5.2	33.9	50,000	18.0	63.5

Table 2b
Core Impedance of the Nickel 200 Ring in Air

Frequency (Hz)	Resistance (ohms)	Reactance (ohms)	Frequency (Hz)	Resistance (ohms)	Reactance (ohms)
500	1.0	1.0	25,500	12.8	50.4
1,000	1.0	2.2	26,000	13.4	51.4
1,500	1.0	3.4	26,500	13.8	52.2
2,000	1.0	4.5	27,000	14.2	53.0
2,500	1.0	5.7	27,500	14.5	53.9
3,000	1.1	6.9	28,000	14.9	54.7
3,500	1.2	8.1	28,500	15.4	55.6
4,000	1.3	9.4	29,000	15.9	56.4
4,500	1.4	10.5	29,500	16.4	57.2
5,000	1.6	11.7	30,000	16.8	58.0
5,500	1.7	13.0	30,500	17.4	58.9
6,000	1.9	14.2	31,000	17.8	59.8
6,500	2.1	15.4	31,500	18.4	60.5
7,000	2.3	16.6	32,000	18.9	61.4
7,500	2.5	18.0	32,500	19.4	62.2
8,000	2.8	19.5	33,000	19.9	62.8
8,500	3.1	20.8	33,500	20.4	63.7
9,000	3.5	22.4	34,000	20.9	64.4
9,500	4.0	24.3	34,500	21.4	65.3
10,000	4.7	26.8	35,000	22.0	66.0
10,500	5.4	30.6	35,500	22.5	66.8
11,000	9.9	40.2	36,000	23.0	67.6
11,500	86.6	-44.5	36,500	23.6	68.3
12,000	1.6	8.5	37,000	24.3	69.0
12,500	2.3	17.9	37,500	24.6	69.6
13,000	3.0	21.7	38,000	25.1	70.4
13,500	3.5	24.0	38,500	25.7	71.2
14,000	3.9	25.9	39,000	26.1	71.9
14,500	4.3	27.6	39,500	26.7	73.6
15,000	4.6	29.0	40,000	27.3	73.3
15,500	5.0	30.2	40,500	27.7	74.0
16,000	5.4	31.5	41,000	28.3	74.8
16,500	5.8	32.5	41,500	28.9	75.3
17,000	6.0	33.8	42,000	29.5	76.1
17,500	6.4	34.8	42,500	30.0	76.8
18,000	6.8	35.8	43,000	30.7	77.4
18,500	7.2	36.8	43,500	31.2	78.1
19,000	7.5	38.0	44,000	31.7	78.7
19,500	7.9	38.9	44,500	32.3	79.4
20,000	8.3	39.9	45,000	32.9	80.0
20,500	8.7	40.9	45,500	33.5	80.6
21,000	9.0	41.9	46,000	34.1	81.3
21,500	9.4	42.9	46,500	34.7	81.9
22,000	9.8	43.8	47,000	35.2	82.6
22,500	10.2	44.8	47,500	35.8	83.2
23,000	10.6	45.7	48,000	36.4	83.8
23,500	11.0	46.6	48,500	37.1	84.3
24,000	11.5	47.7	49,000	37.7	85.1
24,500	11.9	48.5	49,500	38.2	85.6
25,000	12.4	49.4	50,000	38.5	86.0

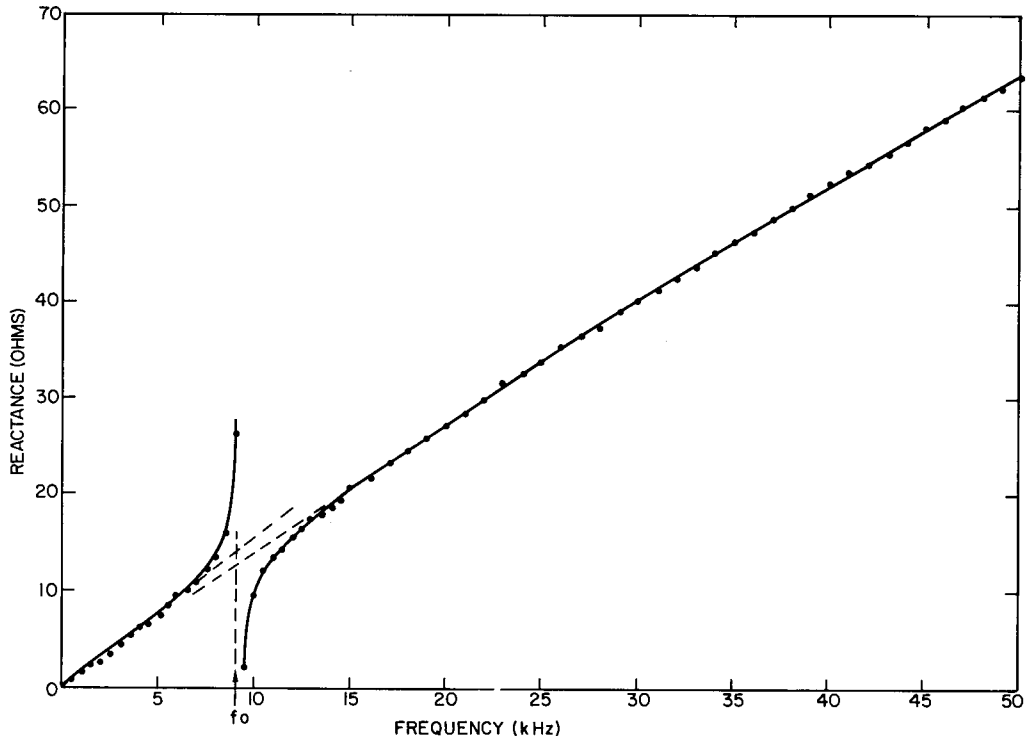


Fig. 4a — Core reactance of the CTN (INCO cube-textured nickel) ring in air

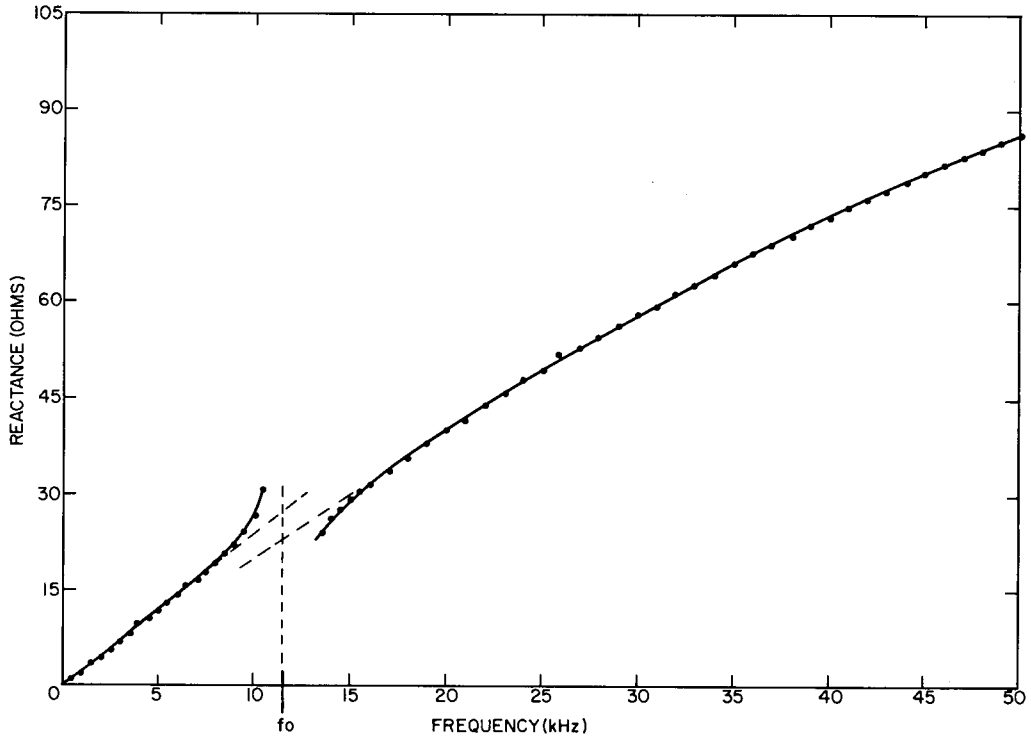


Fig. 4b — Core reactance of the Nickel 200 ring in air

Table 3a
Impedance of the CTN Ring
Near Air Resonance

Frequency (Hz)	Resistance (ohms)	Reactance (ohms)
8,000	1.5	13.6
8,500	2.0	16.0
9,000	5.5	26.2
9,100	13.0	36.6
9,136	23.7	43.9
9,144	27.5	45.4
9,146	29.3	45.9
9,150	32.1	46.7
9,153	34.5	46.9
9,156	36.7	47.1
9,159	39.9	47.2
9,162	44.7	46.9
9,169	50.2	45.0
9,175	58.9	40.2
9,178	62.7	37.3
9,181	65.3	34.8
9,184	69.0	30.3
9,188	72.3	24.3
9,192	74.7	17.0
9,195	75.4	12.6
9,197	75.5	7.0
9,199	75.1	4.0
9,202	74.0	-1.1
9,204	72.6	-5.0
9,206	70.8	-8.8
9,210	68.8	-12.5
9,212	66.3	-15.8
9,215	62.9	-19.4
9,220	58.4	-23.1
9,222	56.5	-24.6
9,225	52.9	-26.3
9,229	49.2	-27.7
9,232	46.3	-28.7
9,235	42.9	-29.2
9,237	40.9	-29.5
9,239	39.3	-29.6
9,241	36.9	-29.6
9,243	35.1	-29.5
9,246	33.2	-29.3
9,249	30.7	-28.9
9,268	19.9	-25.1
9,278	16.4	-22.9
9,306	9.1	-15.8
9,352	4.6	-8.5
9,425	2.1	-1.5
9,500	1.4	+2.0

Table 3b
Impedance of the Nickel 200 Ring
Near Air Resonance

Frequency (Hz)	Resistance (ohms)	Reactance (ohms)
10,500	5.4	30.6
11,000	9.9	40.2
11,100	12.7	44.6
11,200	18.4	51.3
11,300	33.1	62.2
11,350	51.9	68.1
11,365	60.2	68.9
11,379	69.4	67.7
11,386	75.3	66.4
11,393	82.0	64.1
11,400	87.3	61.6
11,408	94.3	57.0
11,412	98.0	54.2
11,418	102.4	50.0
11,423	106.8	44.7
11,429	110.9	38.7
11,436	115.4	28.7
11,443	117.9	20.1
11,450	118.9	10.7
11,456	118.5	1.6
11,458	118.2	-1.1
11,460	117.7	-3.7
11,462	117.0	-6.8
11,464	116.3	-8.9
11,466	115.6	-11.2
11,469	113.7	-16.1
11,474	110.7	-21.7
11,478	107.3	-27.0
11,484	102.3	-32.9
11,490	96.2	-38.3
11,498	88.5	-43.4
11,502	84.6	-45.5
11,507	78.7	-47.9
11,510	75.1	-48.9
11,517	69.3	-50.3
11,520	65.9	-50.8
11,523	62.9	-50.9
11,526	60.2	-51.1
11,528	58.6	-51.0
11,530	57.3	-50.9
11,532	54.4	-50.8
11,537	51.1	-50.4
11,541	47.4	-49.7
11,545	44.4	-48.9
11,550	41.4	-47.9
11,551	40.5	-47.7
11,557	36.9	-46.3
11,571	29.6	-42.4
11,594	20.9	-35.7
11,625	13.4	-27.2
11,661	8.4	-19.0
11,718	4.5	-9.9
11,803	2.3	-1.1

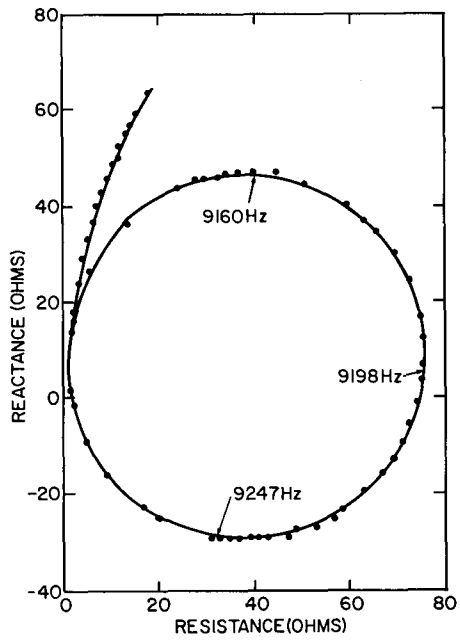


Fig. 5a — Electrical input impedance of the CTN ring near air resonance

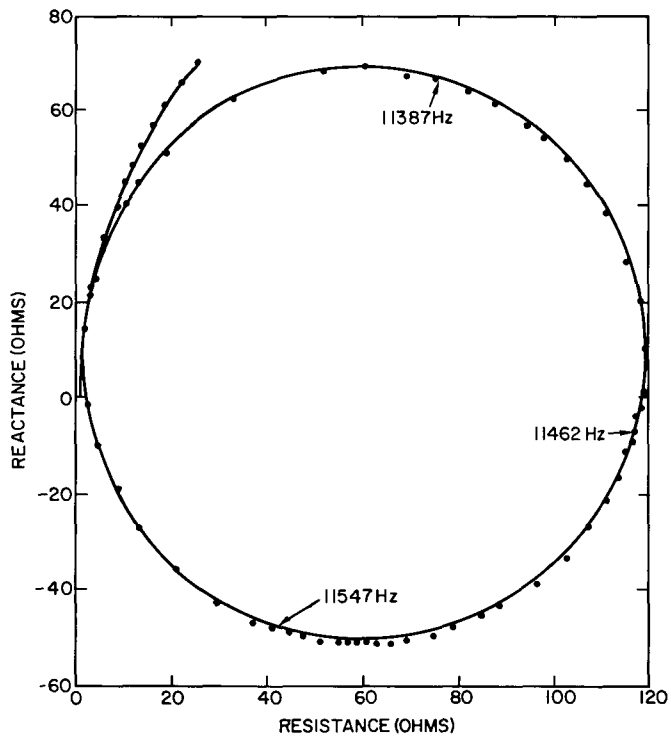


Fig. 5b — Electrical input impedance of the Nickel 200 ring near air resonance

Table 4a
Impedance of the CTN Ring Near
Water Resonance

Table 4b
Impedance of the Nickel 200 Ring Near
Water Resonance

Frequency (Hz)	Resistance (ohms)	Reactance (ohms)	Frequency (Hz)	Resistance (ohms)	Reactance (ohms)
6,000	1.0	9.1	9,000	7.2	24.1
6,500	1.3	10.3	9,040	7.7	24.2
7,000	2.2	12.1	9,069	7.9	24.3
7,100	2.6	12.5	9,078	8.1	24.3
7,150	3.0	12.8	9,096	8.3	24.4
7,200	3.3	13.0	9,103	8.3	24.3
7,250	3.7	13.2	9,122	8.5	24.4
7,270	3.9	13.2	9,144	8.8	24.4
7,303	4.3	13.3	9,168	9.1	24.4
7,322	4.5	13.4	9,187	9.3	24.4
7,348	4.9	13.3	9,202	9.6	24.3
7,396	5.6	13.3	9,229	9.9	24.2
7,435	6.0	13.2	9,261	10.4	24.2
7,460	6.4	13.0	9,289	10.9	24.0
7,488	6.8	12.7	9,318	11.3	23.8
7,501	7.0	12.5	9,351	11.8	23.5
7,532	7.3	12.1	9,379	12.2	23.2
7,554	7.5	11.8	9,420	12.8	22.7
7,570	7.6	11.6	9,465	13.3	22.0
7,583	7.7	11.3	9,497	13.6	21.4
7,592	7.7	11.1	9,518	13.8	21.0
7,601	7.8	11.0	9,558	13.9	20.2
7,614	7.8	10.7	9,575	14.0	19.8
7,628	7.8	10.5	9,598	14.1	19.4
7,642	7.8	10.3	9,621	14.0	18.9
7,658	7.8	9.9	9,648	13.9	18.4
7,668	7.7	9.8	9,709	13.5	17.2
7,689	7.6	9.4	9,741	13.1	16.5
7,711	7.5	9.1	9,795	12.4	15.8
7,733	7.3	8.8	9,832	11.9	15.4
7,769	7.0	8.4	9,892	11.0	14.8
7,786	6.8	8.1	9,921	10.5	14.7
7,804	6.6	7.9	9,942	10.2	14.6
7,824	6.4	7.8	9,961	9.9	14.5
7,838	6.2	7.7	9,978	9.7	14.5
7,854	6.0	7.6	9,993	9.4	14.5
7,867	5.9	7.6	10,025	9.0	14.5
7,890	5.6	7.5	10,054	8.6	14.5
7,902	5.4	7.4	10,085	8.3	14.6
7,917	5.3	7.3	10,114	7.9	14.6
7,930	5.2	7.3	10,140	7.6	14.7
7,942	5.0	7.3	10,558	4.7	16.6
7,954	4.9	7.3	11,037	3.4	19.0
7,970	4.7	7.3			
7,982	4.6	7.3			
8,002	4.4	7.3			
8,044	4.0	7.4			
8,100	3.6	7.5			
8,201	3.0	7.9			
8,308	2.6	8.3			
8,400	2.3	8.6			
8,500	2.0	9.1			
8,600	1.8	9.3			
8,700	1.7	9.6			
8,800	1.6	10.0			
8,900	1.5	10.2			
9,000	1.5	10.4			
9,500	1.4	11.5			
10,000	1.4	12.4			

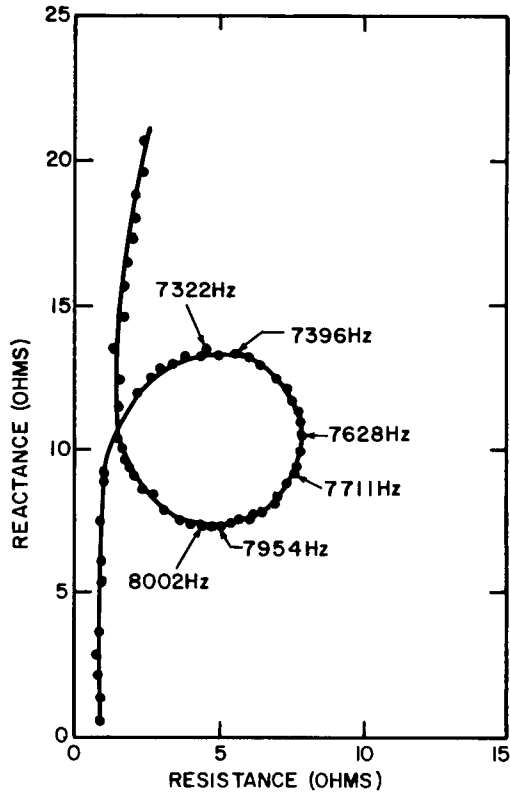


Fig. 6a — Electrical input impedance of the CTN ring in water

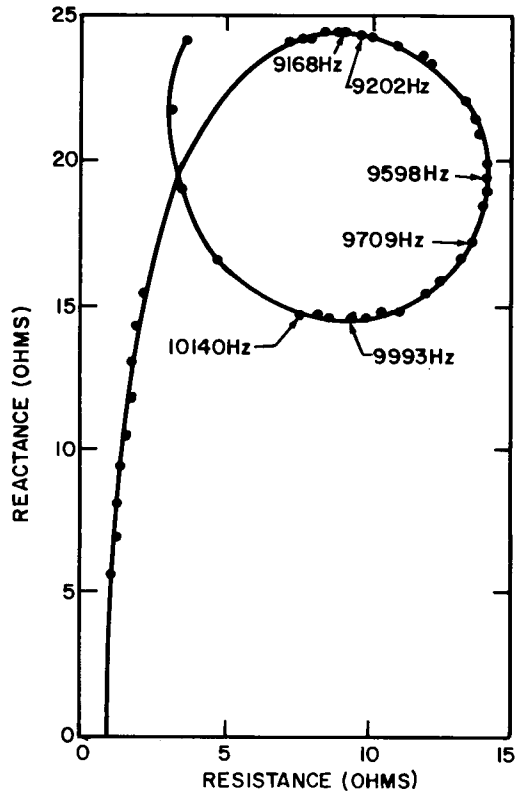


Fig. 6b — Electrical input impedance of the Nickel 200 ring in water

Figure 7a shows the transmitting-current response of the CTN ring, and Fig. 7b shows the transmitting-current response of the Nickel 200 ring. The response is for two angular orientations, radial and axial, of each ring with respect to the hydrophone. The radial response was taken with the hydrophone on an extended radius of the ring and 2.5 meters from the center, and the axial response was taken with the hydrophone on the axis of the ring and 2.5 meters from the center. Selected far-field plots corresponding to interesting features of the frequency response of the Nickel 200 ring appear in Fig. 8. These plots are directivity patterns which are not plotted against the same absolute scale. The recorded pressure level at 0 degrees was arbitrarily adjusted for each plot. Consequently the relative pressure magnitude as a function of angular orientation of the ring at one of the designated frequencies of excitation may be determined from the plots, but the relative pressure magnitude as a function of the frequencies of excitation for a specific angular orientation of the ring may not be determined by a comparison of the plots in Fig. 8. Comparison as a function of frequency is however available from Fig. 7a in conjunction with Fig. 8.

ANALYSIS

An approximate analytical expression which relates the in-air total electrical impedance measured at a transducer's input terminals and the transducer material parameters is

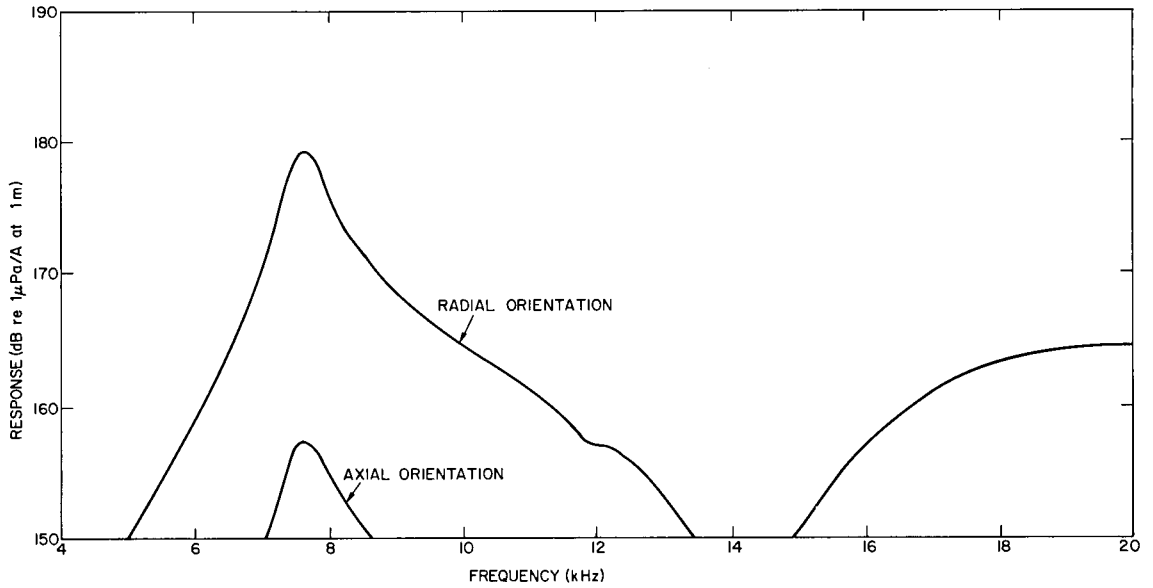


Fig. 7a — Far-field transmitting-current response of the CTN ring

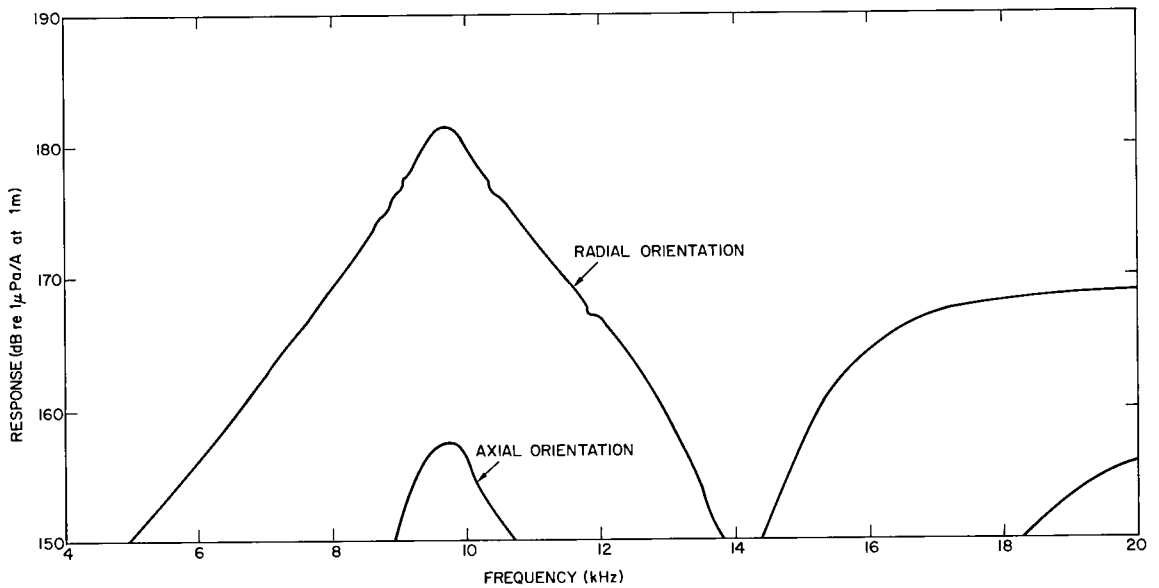
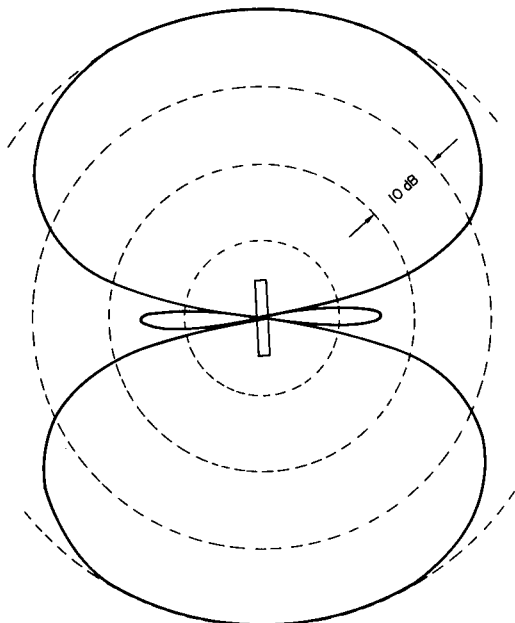
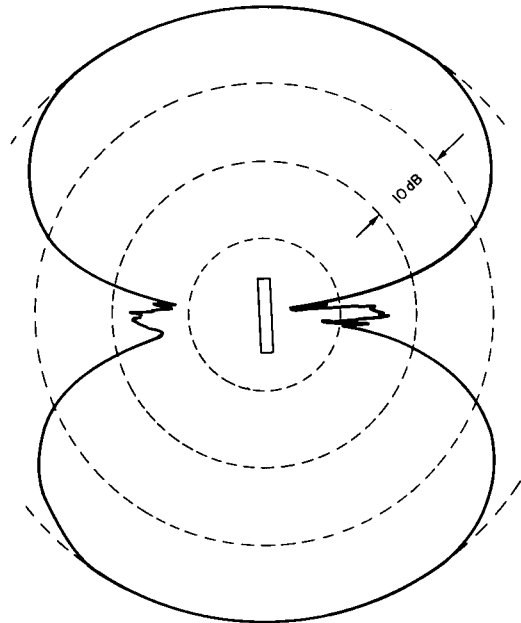


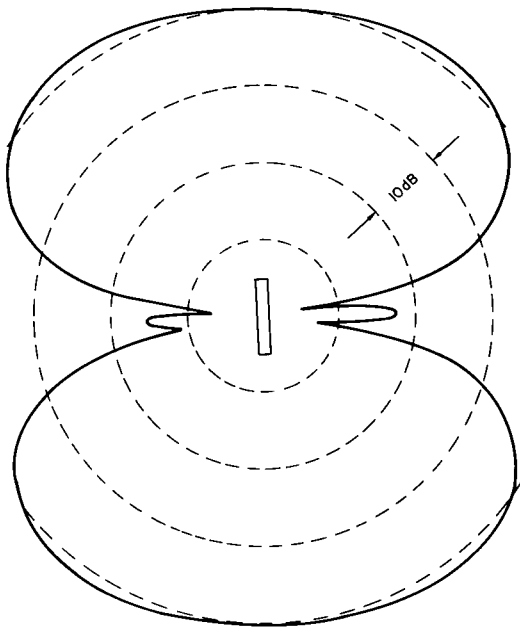
Fig. 7b — Far-field transmitting-current response of the Nickel 200 ring



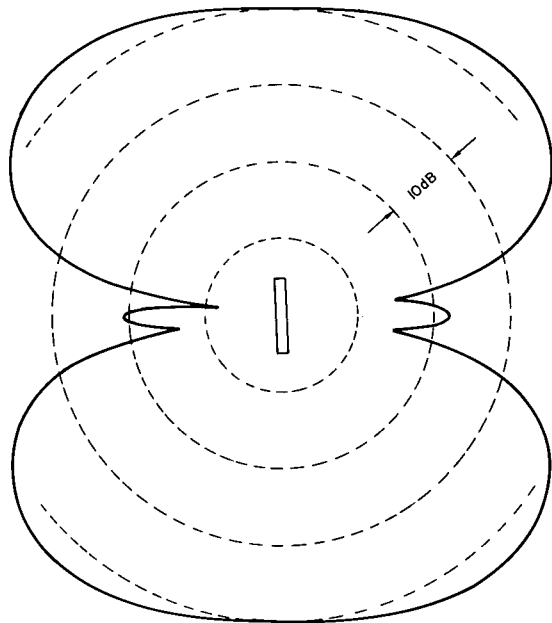
(a) At 9 kHz



(b) At 9.7 kHz



(c) At 11 kHz



(d) At 12 kHz

Fig. 8 — Directivity patterns of the Nickel 200 ring

needed to extract the material parameters from the measurements. These calculated parameters can then be inserted into an appropriate theoretical model of a magnetostrictive ring and the in-water behavior of the ring transducer can be predicted. In addition a theoretical model provides a design capability for a magnetostrictive ring transducer of different dimensions with the same material parameters. An approximate expression for the total electrical input impedance Z_T of a magnetostrictive ring transducer in air is derived as a function of the electrical and magnetostrictive properties and the dimensions of the ring from Butterworth and Smith's equivalent circuit of a single-degree-of-freedom (one-dimensional) magnetostrictive oscillator [5]:

$$Z_T = r_w + \frac{jfN^2 4\pi 10^{-7}}{a} (A_{\text{coil}} - A_0) + \frac{jfN^2 \mu_{33}^S A_0 \chi}{a} + \left(\frac{\mu_{33}^S N g_{33} A_0 \chi}{a S_{33}^B} \right)^2 \left(\frac{1}{R_m + jX_m} \right), \quad (1)$$

where

$$R_m = R_{mp} + \frac{A_0 k_{33}^2 \chi_I}{af S_{33}^B}$$

and

$$X_m = 2\pi f M - \frac{A_0 (1 - k_{33}^2 \chi_R)}{af S_{33}^B}.$$

This expression for Z_T is written in a form compatible with all of the variables in MKS units. The symbols chosen for the material constants are consistent with the "IEEE Standard on Magnetostrictive Materials" [6]. The term r_w is primarily the dc resistance of the toroidal windings and is typically less than 1 ohm. The second term on the right, which Butterworth and Smith neglect, represents the leakage magnetic flux and is negligible if the cross-sectional area of the windings A_{coil} is not much greater than the cross-sectional area of the core A_0 and if the reversible permeability of the core is large compared to that of air and water. In this experiment this leakage-flux term must be included, because it is not negligible with respect to the total impedance off resonance. The first three terms on the right are independent of the magnetostrictive and motional properties of the ring. They represent the core impedance that would be obtained if the ring could be rigidly clamped. The fourth (last) term on the right is the motional impedance term.

In this equation f is the frequency of oscillation, N is the number of turns of wire around the core, μ_{33}^S is the reversible permeability at constant strain, χ is the eddy current vector, χ_I is the imaginary part of χ , χ_R is the real part of χ , a is the mean radius of the core (assuming that the thickness of the core is small compared to the diameter), g_{33} is the piezomagnetic constant relating circumferential strain and circumferential magnetic induction in the ring core, M is the mass of the ring core, S_{33}^B is the elastic

compliance at constant magnetic induction of the ring core, k_{33} is the material electro-mechanical coupling coefficient, R_m and X_m are the mechanical resistance and reactance of the core, and R_{mp} is the portion of the mechanical resistance corresponding to losses in the core other than eddy current and hysteresis losses.

The eddy-current factor is defined [7] as

$$\chi = \chi_0 e^{-jk} = \chi_R - j\chi_I,$$

and the tangent of the loss angle ζ is $\tan \zeta = \chi_I/\chi_R$.

The angle between the resonance diameter of the total impedance circle (the diameter of the circle joining the core impedance and impedance at the resonance frequency) and the horizontal represents the eddy currents and hysteresis in the ring core for in-air excitation. The angle is twice the sum of ζ , an angle corresponding to eddy current losses, and η , an angle corresponding to hysteresis losses. The total angle of impedance-circle tilt is measured from the plots in Figs. 5a and 5b, and the difference between 1/2 the total angles measured and ζ is η .

The material properties of the CTN ring and the Nickel 200 ring which are derived from the in-air impedance measurements are the elastic compliance S_{33}^B , the reversible permeability at constant stress μ_{33}^T , the material electromechanical coupling coefficient k_{33} , and the piezomagnetic strain constant g_{33} .

The reversible permeability is obtained from a plot of the low-frequency core reactance versus frequency. At frequencies of excitation of a ring well below the radial resonance frequency, the motional impedance of the ring is negligible and the total reactance is given by the core reactance:

$$X_c = \frac{fN^2 4\pi 10^{-7}}{a} (A_{\text{coil}} - A_0) + \frac{fN^2 \mu_{33}^T A_0}{a},$$

where μ_{33}^T is the reversible permeability at constant stress. In this experiment χ_R , the real part of χ , is assumed to be unity for the ring cores, because the rings' metal strip thickness is much less than the wavelength of sound in the material over the frequency range of interest. The slope of a plot of X_c versus f is given by

$$\begin{aligned} \frac{dX_c}{df} &= \frac{N^2 4\pi 10^{-7}}{a} (A_{\text{coil}} - A_0) + \frac{N^2 \mu_{33}^T A_0}{a} \\ &= \frac{N^2 4\pi 10^{-7}}{a} \left[A_{\text{coil}} + \left(\frac{\mu_{33}^T}{4\pi 10^{-7}} - 1 \right) A_0 \right]. \end{aligned}$$

Therefore

$$\mu_{33}^T = \frac{a}{A_0 N^2} \frac{dX_c}{df} + \left(1 - \frac{A_{\text{coil}}}{A_0} \right) 4\pi 10^{-7}. \quad (2)$$

The reversible permeability at constant strain is related to the relative permeability at constant stress by

$$\mu_{33}^S = \mu_{33}^T (1 - k_{33}^2).$$

The effective electromechanical coupling coefficient k is calculated from

$$\frac{k^2}{1 - k^2} = \frac{D_z}{Q_z X_b}, \quad (3)$$

where D_z is the diameter of the motional impedance circle in ohms, Q_z is the quality factor of the transducer, and X_b is the core reactance at the radial resonance frequency. The core reactance at radial resonance is difficult to determine, because it cannot be measured directly. It was therefore estimated from plots of core reactance versus frequency well below resonance and well above resonance. The off-resonance curves were extrapolated to the radial resonance frequency, and X_b was bounded by the extrapolated curves. This method of determining core reactance at resonance is complicated by the frequency-dependent hysteresis and eddy-current losses in the ring, which tend to cause the curve to increasingly depart from a straight line at increasing frequencies. The magnitude of core impedance at resonance was then obtained from the plot of total input electrical reactance versus total input electrical resistance as the magnitude of the impedance vector corresponding to the estimated core reactance. The motional impedance is the total input electrical impedance minus the core impedance. The core impedance was assumed to be constant for the purpose of the in-air motional impedance calculations because the in-air Q values of the rings used in the experiment were large and therefore the range of frequencies corresponding to nonnegligible motional impedances was small. The quality factor of a ring transducer is

$$Q_z = \frac{f_0}{f_2 - f_1},$$

where f_0 , the radial resonance frequency, is the frequency corresponding to maximum motional impedance and f_2 and f_1 , the quadrantal frequencies, are the frequencies corresponding to a motional impedance whose magnitude is 0.707 times the magnitude of the maximum motional impedance. The diameter D_z was measured directly from the plotted motional impedance circles.

The electromechanical coupling coefficient k is the effective coupling coefficient of the ring transducer with leakage inductance present. Although this coupling coefficient is important in transducer applications as an index of performance potential, in material measurements it serves only as an intermediary in the calculation of more basic parameters. The material electromechanical coupling coefficient k_{33} is given [8] by

$$k_{33}^2 = \frac{k^2}{1 - \frac{L_0}{L_f} \left(1 - \frac{A_0}{A_{\text{coil}}} \right)},$$

where L_0 is the inductance of the winding with the ring core removed and L'_f is the free inductance measured at frequencies well below the ring radial resonance frequency:

$$L_0 = \frac{N^2 4\pi 10^{-7} A_{\text{coil}}}{2\pi a} .$$

with the assumption $\chi \approx 1$,

$$L'_f = \frac{N^2 4\pi 10^{-7} (A_{\text{coil}} - A_0)}{2\pi a} + \frac{N^2 \mu_{33}^T A_0}{2\pi a} .$$

Therefore,

$$k_{33}^2 = \frac{k^2}{\frac{A_{\text{coil}}}{A_0} - 1} \cdot \frac{1}{1 - \frac{A_{\text{coil}}}{A_0} - 1 + \left(\frac{\mu_{33}^T}{4\pi 10^{-7}} \right)} . \quad (4)$$

The piezomagnetic strain constant g_{33} is derived in terms of k_{33} , μ_{33}^T , and S_{33}^B from the small-signal linear piezomagnetic transducer equations [1, 9]:

$$g_{33} = \frac{k_{33}}{\sqrt{1 - k_{33}^2}} \sqrt{\frac{S_{33}^B}{\mu_{33}^T}} . \quad (5)$$

All of the variables on the right are known from previous calculations except S_{33}^B , the elastic compliance. The elastic compliance is calculated from the motional impedance term in Eq. (1). For $\chi \approx 1$ the motional impedance is a maximum when the mechanical reactance X_m goes to zero. This occurs, by definition, at the radial resonance frequency f_0 :

$$X_m = 0 = 2\pi f_0 M - \frac{A_0(1 - k_{33}^2)}{af_0 S_{33}^B}$$

or

$$S_{33}^B = \frac{(1 - k_{33}^2)A_0}{2\pi M f_0^2 a} . \quad (6)$$

Young's modulus E at constant magnetic induction field is the reciprocal of S_{33}^B .

CALCULATIONS

The relative reversible permeability μ_{33}^T was calculated from Eq. (2). For the CTN ring

$$A_0 = 1.349 \times 10^{-4} \text{ m}^2,$$

$$A_{\text{coil}} = 1.219 \times 10^{-3} \text{ m}^2,$$

and

$$\mu_{33\text{CTN}}^T = \left(1.87 \times 10^4 \left. \frac{dX_c}{df} \right|_{\text{CTN}} + 1 - 9.036 \right) 4\pi \times 10^{-7}.$$

In Fig. 4a, $dX_c/df|_{\text{CTN}}$ is the slope of the low-frequency linear portion of the curve:

$$\left. \frac{dX_c}{df} \right|_{\text{CTN}} = (1.52 \pm 0.02) \times 10^{-3} \text{ ohm/hertz}.$$

Therefore,

$$\mu_{33\text{CTN}}^T = (20.4 \pm 0.4) 4\pi \times 10^{-7} \text{ newton/ampere}^2.$$

For the Nickel 200 ring

$$A_0 = 1.253 \times 10^{-4} \text{ m}^2,$$

$$A_{\text{coil}} = 1.070 \times 10^{-3} \text{ m}^2,$$

and

$$\mu_{33\text{Ni200}}^T = \left(2.01 \times 10^4 \left. \frac{dX_c}{df} \right|_{\text{Ni200}} + 1 - 8.540 \right) 4\pi \times 10^{-7}.$$

In Fig. 4b, $dX_c/df|_{\text{Ni200}}$ is the slope of the low-frequency linear portion of the curve:

$$\left. \frac{dX_c}{df} \right|_{\text{Ni200}} = (2.40 \pm 0.02) \times 10^{-3} \text{ ohm/hertz}.$$

Therefore,

$$\mu_{33\text{Ni200}}^T = (40.7 \pm 0.4) 4\pi \times 10^{-7} \text{ newton/ampere}^2.$$

The value of core reactance at ring radial resonance X_b is estimated for each ring from Figs. 4a and 4b. Figure 5a shows that the radial resonance frequency of the CTN ring (the frequency corresponding to maximum motional impedance) is approximately 9.2 kHz. At 9.2 kHz the core reactance from Fig. 4a is undetermined in the range

$$12.7 \pm 0.2 \leq X_{b_{\text{CTN}}} \leq 14.0 \pm 0.2 \text{ ohms.}$$

(The extrapolated high-frequency portion of the curve in Fig. 4a has the value 12.7 ± 0.2 ohms at f_0 and the extrapolated low frequency portion of the curve has the value 14.0 ± 0.2 ohms at f_0 .) For the Nickel 200 ring the radial resonance frequency is approximately 11.5 kHz. The core reactance at this frequency is undetermined in Fig. 4b in the range

$$22.8 \pm 0.2 \leq X_{b_{\text{Ni200}}} \leq 27.2 \pm 0.2 \text{ ohms.}$$

The relative uncertainty ($\approx 20\%$) in X_b for the Nickel 200 ring is approximately twice as large as the relative uncertainty ($\approx 10\%$) in X_b for the CTN ring, which roughly corresponds to the ratio of the permeabilities of the rings. The much smaller core resistances at the rings' radial resonances were similarly extrapolated from the data in Tables 2a and 2b. Using an average core reactance for the CTN ring of 13.4 ohms and a core resistance of 1.2 ohms, the motional impedance of the CTN ring was calculated at all frequencies near air resonance (Table 5a and Fig. 9a). The slight departure of the data points from a circle near maximum motional resistance is characteristic of all of the CTN rings that have been investigated. Maximum motional impedance of the CTN ring is 74.6 ohms and corresponds to 9198 ± 1 Hz. The quadrantal frequencies were 9160 ± 1 Hz and 9247 ± 1 Hz. Thus

$$Q_{z_{\text{CTN}}} = \frac{9198}{9247 - 9160} = 106 \pm 2.$$

The diameter of the motional impedance circle is $76.5 \pm_{-1.9}^{+1.4}$ ohms, and the tilt of the circle is 6.0 ± 0.5 degrees when reckoned from the average core reactance of 13.4 ohms. Using an average core reactance for the Nickel 200 ring of 25.0 ohms and a core resistance of 3.2 ohms, the motional impedance was calculated at all frequencies near air resonance (Table 5b and Fig. 9b). Maximum motional impedance of the Nickel 200 ring is 118.2 ohms and corresponds to 11462 ± 1 Hz. The quadrantal frequencies were 11387 ± 1 Hz and 11547 ± 1 Hz. Thus

$$Q_{z_{\text{Ni200}}} = \frac{11462}{11547 - 11387} = 71.6 \pm 1.$$

The diameter of the motional impedance circle is 119 ± 1.4 ohms, and the tilt of the circle is 15.5 ± 0.5 degrees when reckoned from the average core reactance of 25.0 ohms.

The effective electromechanical coupling coefficient k was calculated for each ring from Eq. (3) using the experimentally determined values of D_z , X_b , and Q_z . For the CTN ring

Table 5a
Calculated Motional Impedance of the
CTN Ring Near Air Resonance

Table 5b
Calculated Motional Impedance of the
Nickel 200 Ring Near Air Resonance

Frequency (Hz)	Resistance (ohms)	Reactance (ohms)	Frequency (Hz)	Resistance (ohms)	Reactance (ohms)
8,000	0.45	2.0	10,500	2.7	7.9
8,500	0.85	3.6	11,000	6.9	16.3
9,000	4.3	13.1	11,100	9.7	20.4
9,100	11.8	23.4	11,200	15.4	26.9
9,136	22.5	30.6	11,300	30.0	37.6
9,144	26.3	32.1	11,350	48.8	43.4
9,146	28.1	32.6	11,365	57.1	44.2
9,150	30.9	33.4	11,379	66.3	43.0
9,153	33.3	33.6	11,386	72.2	41.7
9,156	35.5	33.8	11,393	78.9	39.4
9,159	38.7	33.9	11,400	84.2	36.8
9,162	43.5	33.6	11,408	91.2	32.2
9,169	49.0	31.7	11,412	94.9	29.4
9,175	57.7	26.9	11,418	99.3	25.2
9,178	61.5	23.9	11,423	103.7	19.9
9,181	64.1	21.4	11,429	107.8	13.9
9,184	67.8	16.9	11,436	112.3	3.9
9,188	71.1	10.9	11,443	114.8	-4.7
9,192	73.5	3.6	11,450	115.8	-14.2
9,195	74.2	-0.8	11,456	115.4	-23.3
9,197	74.3	-6.4	11,458	115.1	-26.0
9,199	73.9	-9.4	11,460	114.6	-28.6
9,202	72.8	-14.5	11,462	113.9	-31.7
9,204	71.4	-18.4	11,464	113.2	-33.8
9,206	69.6	-22.2	11,466	112.5	-36.1
9,210	67.6	-25.9	11,469	110.6	-41.0
9,212	65.1	-29.2	11,474	107.6	-46.6
9,215	61.7	-32.8	11,478	104.2	-51.9
9,220	57.2	-36.5	11,484	99.2	-57.8
9,222	55.3	-38.0	11,490	93.1	-63.2
9,225	51.7	-39.7	11,498	85.4	-68.3
9,229	48.0	-41.6	11,502	81.4	-70.5
9,232	45.1	-42.2	11,507	75.5	-72.9
9,235	41.7	-42.7	11,510	71.9	-73.9
9,237	39.7	-43.0	11,517	66.1	-75.3
9,239	38.1	-43.1	11,520	62.7	-75.8
9,241	35.7	-43.1	11,523	59.7	-75.9
9,243	33.9	-43.0	11,526	57.0	-76.1
9,246	32.0	-42.8	11,528	55.4	-76.0
9,249	29.5	-42.4	11,530	54.1	-75.9
9,268	18.7	-38.7	11,532	51.2	-75.8
9,278	15.2	-36.4	11,537	47.9	-75.4
9,306	7.9	-29.4	11,541	44.2	-74.7
9,352	3.4	-22.1	11,545	41.2	-73.9
9,425	0.9	-15.2	11,550	37.9	-73.0
9,500	0.2	-11.7	11,551	37.3	-72.8
			11,557	33.7	-71.4
			11,571	26.4	-67.5
			11,594	17.7	-60.8
			11,625	10.2	-52.4
			11,661	5.2	-44.2
			11,718	1.2	-35.3
			11,803	-1.0	-26.7

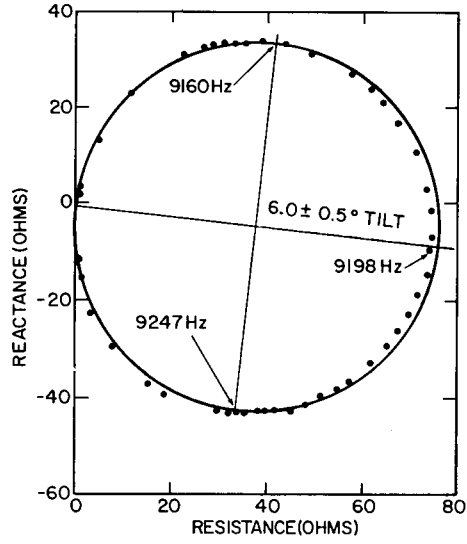


Fig. 9a — Calculated motional impedance of the CTN ring

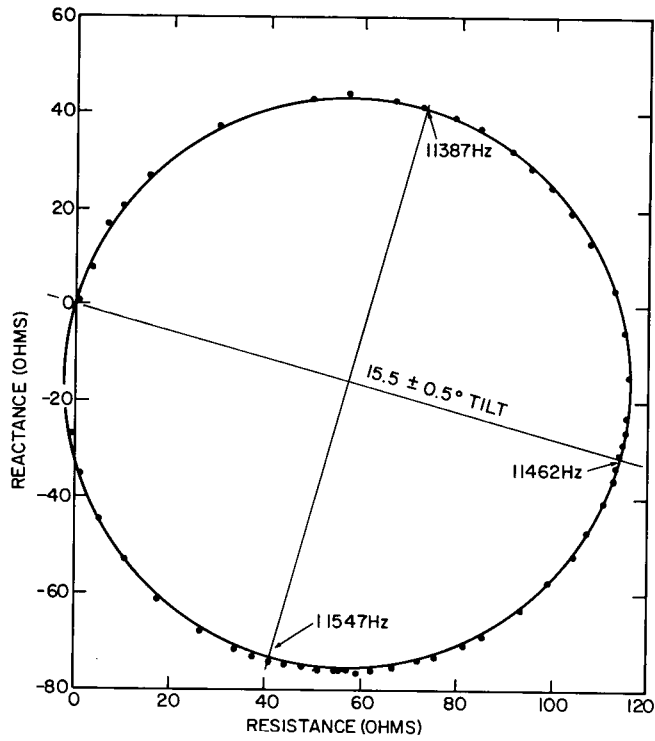


Fig. 9b — Calculated motional impedance of the Nickel 200 ring

JOEL A. SINSKY

$$\frac{k^2}{1 - k^2} = \frac{76.5}{(106)(13.4)}$$

or

$$k_{\text{CTN}} = 0.226.$$

For the Nickel 200 ring

$$\frac{k^2}{1 - k^2} = \frac{119}{(71.6)(25.0)}$$

or

$$k_{\text{Ni200}} = 0.250.$$

The material electromechanical coupling coefficient k_{33} was calculated for each ring from Eq. (4). For the CTN ring

$$\frac{A_{\text{coil}}}{A_0} = 9.036,$$

$$\mu_{33}^T = 20.4 \times 4\pi \times 10^{-7} \text{ newton/ampere}^2,$$

and

$$k_{33}^2 = \frac{(0.226)^2}{1 - \frac{9.036 - 1}{9.036 - 1 + 20.4}}$$

or

$$k_{33\text{CTN}} = 0.267.$$

For the Ni 200 ring

$$\frac{A_{\text{coil}}}{A_0} = 8.540,$$

$$\mu_{33}^T = 40.7 \times 4\pi \times 10^{-7} \text{ newton/ampere}^2,$$

and

$$k_{33}^2 = \frac{(0.250)^2}{1 - \frac{8.540 - 1}{8.540 - 1 + 40.7}}$$

or

$$k_{33\text{Ni200}} = 0.272.$$

The elastic compliance for each ring was calculated from Eq. (6). For the CTN ring

$$M = 0.4591 \text{ kg}$$

and

$$S_{33}^B{}_{\text{CTN}} = \frac{[1 - (0.267)^2][1.349 \times 10^{-4}]}{2\pi(0.4591)(9198)^2(0.06578)} = 7.80 \times 10^{-12} \text{ m}^2/\text{newton}.$$

Young's modulus E at constant magnetic induction field is

$$E_{\text{CTN}} = \frac{1}{7.80 \times 10^{-12}} = 1.28 \times 10^{11} \text{ newtons/m}^2.$$

For the Nickel 200 ring

$$M = 0.4338 \text{ kg}$$

$$S_{33}^B{}_{\text{Ni200}} = \frac{[1 - (0.272)^2][1.253 \times 10^{-4}]}{2\pi(0.4338)(11462)^2(0.06573)} = 4.93 \times 10^{-12} \text{ m}^2/\text{newton},$$

and

$$E_{\text{Ni200}} = \frac{1}{4.93 \times 10^{-12}} = 2.03 \times 10^{11} \text{ newtons/m}^2.$$

The remaining material constant which appears in Eq. (1) is g_{33} . For the CTN ring

$$g_{33}^{\text{CTN}} = \frac{0.267}{\sqrt{1 - (0.267)^2}} \sqrt{\frac{7.80 \times 10^{-12}}{(4\pi \times 10^{-7})20.4}} \\ = 15.3 \times 10^{-5} \text{ ampere/newton}.$$

For the Nickel 200 ring

$$g_{33}^{\text{Ni200}} = \frac{0.272}{\sqrt{1 - (0.272)^2}} \sqrt{\frac{4.93 \times 10^{-12}}{(4\pi \times 10^{-7})40.7}} \\ = 8.78 \times 10^{-5} \text{ ampere/newton}.$$

The total mechanical resistance R_m at resonance can be calculated from Eq. (1), and R_{mp} may then be determined assuming that the eddy current losses at resonance are much greater than the hysteresis losses ($\zeta \gg \eta$). The real part of Z_T in Eq. (1) at resonance ($X_m = 0$) is given by

$$R_T = R_b + \left(\frac{\mu_{33}^S N g_{33} A_0}{a S_{33}^B} \right)^2 \left(\frac{\chi_R^2 - \chi_I^2}{R_m} \right), \quad (7)$$

in which $R_m = R_{mp} + A_0 k_{33}^2 \chi_I / a f_0 S_{33}^B$.

For the CTN ring at resonance

$$R_T = 75.5 \text{ ohms,}$$

$$R_b = 1.2 \text{ ohms,}$$

$$f_0 = 9197 \text{ Hz,}$$

$$g_{33} = 15.3 \times 10^{-5} \text{ ampere/newton,}$$

$$S_{33}^B = 7.81 \times 10^{-12} \text{ m}^2/\text{newton,}$$

$$k_{33} = 0.267,$$

$$\mu_{33}^T = 20.4 \times 4\pi \times 10^{-7} \text{ newton/ampere}^2,$$

$$\mu_{33}^S = \mu_{33}^T (1 - k_{33}^2) = 19.0 \times 4\pi \times 10^{-7} \text{ newton/ampere}^2,$$

$$\chi_R \approx 1,$$

$$2(\zeta + \eta) \approx 2\zeta = 6 \text{ degrees,}$$

$$\chi_I = \tan \zeta = \tan 3^\circ = 0.0524,$$

$$N = 144 \text{ turns,}$$

$$a = 0.06578 \text{ m,}$$

and

$$A_0 = 1.349 \times 10^{-4} \text{ m}^2.$$

Substituting these values into Eq. (7) yields

$$75.5 = 1.2 + \left[\frac{4\pi(19.0 \times 10^{-7})144(15.3 \times 10^{-5})1.349 \times 10^{-4}}{0.06578 (7.81 \times 10^{-12})} \right]^2 \left[\frac{1 - (0.0524)^2}{R_m} \right]$$

or

$$R_m = 256 \text{ kg/s}$$

and

$$R_{mp} = 256 - \frac{1.349 \times 10^{-4} (0.267)^2 (0.0524)}{(0.06578)(9197)(7.81 \times 10^{-12})}$$

$$= 256 - 107 = 149 \text{ kg/s.}$$

For the Nickel 200 ring at resonance

$$R_T = 117 \text{ ohms,}$$

$$R_b = 3.2 \text{ ohms,}$$

$$f_0 = 11462 \text{ Hz,}$$

$$g_{33} = 8.78 \times 10^{-5} \text{ ampere/newton,}$$

$$S_{33}^B = 4.93 \times 10^{-12} \text{ m}^2/\text{newton,}$$

$$k_{33} = 0.272,$$

$$\mu_{33}^T = 40.7 \times 4\pi \times 10^{-7} \text{ newton/ampere}^2,$$

$$\mu_{33}^S = \mu_{33}^T (1 - k_{33}^2) = 37.7 \times 4\pi \times 10^{-7} \text{ newton/ampere}^2,$$

$$\chi_R \approx 1,$$

$$2(\zeta + \eta) \approx 2\zeta = 15.5 \text{ degrees,}$$

$$\chi_I = \tan \zeta = 0.136,$$

$$N = 144 \text{ turns,}$$

$$a = 0.06573 \text{ m,}$$

$$A_0 = 1.253 \times 10^{-4} \text{ m}^2.$$

Substituting these values into Eq. (7) yields

$$117 = 3.2 + \left[\frac{4\pi(37.7 \times 10^{-7})144(8.78 \times 10^{-5})1.253 \times 10^{-4}}{.06573 (4.93 \times 10^{-12})} \right]^2 \left[\frac{1 - (0.136)^2}{R_m} \right]$$

or

$$R_m = 463 \text{ kg/s.}$$

and

$$R_{mp} = 463 - \frac{1.253 \times 10^{-4} (0.272)^2 (0.136)}{(0.06573)(11462)(4.93 \times 10^{-12})}$$

$$= 463 - 339 = 124 \text{ kg/s.}$$

Table 6 is a summary of the transducers' material parameters which have been derived from electrical impedance measurements. These parameters, derived empirically from measurements and a one-dimensional-magnetostrictive-ring mathematical model, were substituted into the computer program NRL EIGSHIP, and the output of the program was compared with experiment (Appendix A).

Table 6
Transducer Parameters Derived from Electrical Impedance Measurements

Ring	μ_{33}^S ($4\pi \times 10^{-7}$ N/A ²)	f_0 (Hz)	Q_z	Circle Tilt 2ξ (degrees)	k	D_z (ohms)	X_b (ohms)	R_b (ohms)	k_{33}	S_{33}^B (10^{-12} m ² /N)	g_{33} (10^{-5} A ² /N)	R_m (kg/s)	R_{mp} (kg/s)
CTN	19.0	9198	106	6.0	0.226	76.5	13.4	1.2	0.267	7.80	15.3	256	149
Nickel 200	37.7	11462	71.6	15.5	0.250	119.0	25.0	3.2	0.272	4.93	8.78	463	124

CONCLUSIONS

This report documents the electrical input impedances and acoustic radiation characteristics of two magnetostrictive free-flooded ring transducers of similar dimensions but of dissimilar materials and (Appendixes A and B) two other magnetostrictive free-flooded ring (cylinder) transducers of the same material but of progressively greater lengths. The data were obtained using the extensive instrumentation for underwater sound transducer analysis associated with the NRL Acoustic Research Tank. The main purpose for performing and documenting these measurements was to provide experimental data in the literature for comparison with theoretical transducer models. There have been in the past many similar measurements on magnetostrictive ring transducers, but no previous effort appears to have been made in one document to carefully describe the experiment, tabulate and plot the data, suggest probable sources of error, and show comparison with theory. The raw numerical data have been provided to allow the reader the option of using other possible procedures for extracting the material parameters from the data.

Appendix A is really a companion discussion to a pair of NRL Reports [10, 11] having in common the main title "Electroacoustic Modeling of Magnetostrictive Shells and Rings". Reference 10 contains the development of the computer-program analysis NRL EIGSHIP of a magnetostrictive ring transducer. The analysis has been applied to the scale-model rings described here, and a comparison of theory and experiment is given in Appendix A. The agreement between theory and experiment is good for the in-air excitation of the rings but not so good for the in-water excitation. Probable sources of error are discussed in Appendix A. The comparison of the experimental data and the theoretical model NRL EIGSHIP is relegated to an appendix to emphasize the intent of this report to provide data for any theoretical model of a magnetostrictive ring transducer and not specifically for NRL EIGSHIP. However the exercise of a comparison was

constructive, because it provided insight into which parameters must be measured or derived to integrate theory and experiment. When a mathematical model is adequately verified by scale-model ring measurements, the model can then be used as a realistic design tool for evaluating the performance characteristics of magnetostrictive rings in the same regime of relative dimensions as the scale models but of much larger size.

A comprehensive manual of ring-transducer technology based on extrapolations of the theoretical predictions of NRL EIGSHIP which were verified by the experiment described in this report will be written and published as a subsequent NRL Report. It will contain magnetostrictive-ring-transducer design and performance criteria represented by parametric curves, convenient formulas, and basic principles. The manual will be a clear and concise compendium of ring-transducer design information intended for use by technology administrators as well as by transducer design engineers.

ACKNOWLEDGMENTS

The author is grateful to S. Hanish, R. Baier, and P. Rogers for many valuable discussions and to B. King for the NRL EIGSHIP computer results. Appreciation is expressed to E. L. Huston of the International Nickel Company, T. Meyers of the Naval Underwater Systems Center, and D. Gregan and D. Dorsey of NRL for assistance in preparing the transducers and to J. Neeley for assistance in taking the measurements.

REFERENCES

1. J.A. Sinsky, "Comparison of a Cube-Textured Nickel and a Nickel-200 Magnetostrictive Ring Transducer," NRL Report 7779, Aug. 1974.
2. S. Hanish, R.V. Baier, B.J. King, P.H. Rogers, and J.A. Sinsky, "A Mathematical Analysis of a Free-Flooded Finite Length Radiating Magnetostrictive Shell," submitted for publication to the Journal of the Acoustical Society of America.
3. J. Chervenak, "A New NRL Acoustic Research Tank Facility," NRL Report 6822, (1969).
4. R.J. Bobber, *Underwater Electroacoustic Measurements*, Washington, D.C., Naval Research Laboratory, 1970, p. 251.
5. S. Butterworth and F.D. Smith, "The Equivalent Circuit of the Magnetostriction Oscillator," *Proc. Phys. Soc.* 43 (No. 2), 166 (1931).
6. Technical Committee on Transducers and Resonators of the IEEE Group on Sonics and Ultrasonics, "IEEE Standard on Magnetostrictive Materials: Piezomagnetic Nomenclature," The Institute of Electrical and Electronics Engineers, 1971.
7. National Defense Research Committee, "The Design and Construction of Magnetostriction Transducers," Volume 13 of the Summary Technical Report of Division 6, NDRC, Washington, D.C., 1946, p. 69.
8. R.S. Woollett, "Electromechanical Evaluation of Magnetostrictive Cylinders by Resonance-Antiresonance Measurements," USN Underwater Sound Laboratory, Research Report 225, Dec. 1953.

9. R.S. Woollett, "Magnetostrictive Material Requirements for Sonar Transducers," *U.S. Navy Journal of Underwater Acoustics* **20** (No. 4), 1970, p. 679.
10. S. Hanish, R.V. Baier, B.J. King, and P.H. Rogers, "Electroacoustic Modeling of Magnetostrictive Shells and Rings, Part I-Mathematical Modeling," NRL Report 7767, Dec. 1974.
11. S. Hanish, R.V. Baier, and B.J. King, "Electroacoustic Modeling of Magnetostrictive Shells and Rings, Part II," NRL Report to be published.

Appendix A

THEORETICAL PREDICTIONS FROM THE COMPUTER PROGRAM NRL EIGSHIP AND COMPARISON WITH EXPERIMENT

The necessary input parameters for NRL EIGSHIP are divided into five categories:

- Cylinder dimensions and properties,
- Scroll tape dimensions and properties,
- Coil winding dimensions,
- External fluid medium properties,
- Quality factors.

The computer program performs an analysis which is considerably more sophisticated than the Butterworth one-dimensional ring model previously used. It treats the ring as a cylinder and calculates its normal modes of oscillation as well as its velocity distribution (velocity of every point on the surface of the ring). Consequently the Poisson ratio of the ring material is needed in addition to the dimensions, mass density, and Young's modulus. Effective mass density, ρ , is computed from the weight and physical dimensions:

$$\rho = \text{weight}/\text{volume} = \text{weight}/2\pi a A_0.$$

Young's modulus is the reciprocal of the compliance S_{33}^B :

$$Y^B = 1/S_{33}^B.$$

The computer program calculates the total complex reversible permeability and the complex permeability due to hysteresis from the physical dimensions, resistivity, impedance-circle dip angle, and low-frequency real reversible permeability of the scroll material from which the ring transducer is consolidated. The remainder of the electromechanical output parameters are calculated from the inputs listed above as well as the number of turns of wire comprising the toroidal windings and their cross-sectional area, the constant-current quality factor, the copper loss in the windings, and a magnetostrictive constant

$$\text{HTT} = g_{33}/S_{33}^B.$$

The ring transducer's surface velocities, surface pressures, radiation impedance, electrical impedance, motional impedance, efficiency, transmitting response, and radiated acoustic power are all calculated in water using the ring parameter inputs, the density of the water, and the sound velocity in the water. Table A1 gives the input parameters to NRL EIGSHIP for the CTN and Nickel 200 rings in the format of the computer program. Most of the notation and parameter definitions are concise and easily understood with the exception of *total dip angle*, which actually means 1/2 the total dip angle.

Table A1
 Input Parameters (in MKS units) for NRL EIGSHIP
 with Computer Language Designation

Parameter	Computer Language	Value	
		CTN Ring	Nickel 200 Ring
Current	DRIVE CUR	1.5×10^{-2}	1.5×10^{-2}
Cylinder Dimensions and Properties			
Mean radius	R MEAN	6.578×10^{-2}	6.573×10^{-2}
Radial thickness	THK	6.65×10^{-3}	6.45×10^{-3}
Axial length	LTH	2.029×10^{-2}	1.942×10^{-2}
Density	RHO	8.234×10^3	8.383×10^3
Poisson's ratio	NU	3.8×10^{-1}	3.1×10^{-1}
Young's modulus at constant magnetic induction	Y	1.28×10^{11}	2.03×10^{11}
Scroll Tape Dimensions and Properties			
Thickness	THST	2.032×10^{-4}	1.778×10^{-4}
Resistivity	RES	7.58×10^{-8}	8.03×10^{-8}
Relative magnetic permeability at constant strain	URS	19.0	37.7
Permeability of free space	UO	1.2566×10^{-6}	1.2566×10^{-6}
Magnetic permeability at constant strain	US	2.39×10^{-5}	4.74×10^{-5}
Piezomagnetic stress constant	HTT	1.96×10^7	1.78×10^7
Total dip angle	DIP	-3.0	-7.75
Coil Winding Dimensions			
Number of turns	NTRN	144	144
Radial thickness \times Axial length	THC \times LC	1.219×10^{-3}	1.070×10^{-3}
Copper loss in coil	REL	8.0×10^{-1}	1.0
External Fluid Medium Properties			
Density	RHOF	1×10^3	1×10^3
Speed of sound	CF	1.482×10^3	1.482×10^3
Quality Factor			
Constant current	QI	1.06×10^2	7.16×10

A computer-program output listing is given for each frequency desired. The reference surface velocity in air and in water is given for a specified number of circumferential bands around the ring. The number of bands chosen is determined by the height of the ring and the complexity of the mode of oscillation. For the rings with relatively short heights described in this report, six bands are adequate (Fig. A1) and the radial breathing mode is predominant. The reference surface is a cylinder of zero thickness whose radius is the mean radius of the ring and whose height is the height of the ring. For an unclamped ring transducer in a free field, the motion of the upper half of the ring and the lower half of the ring are identical. Therefore the bands include the outside upper half and top edge of the reference surface. The inside upper half of the reference surface has the same magnitude of motion as the outside but is shifted 180 degrees in phase. The real part, imaginary part, absolute magnitude, and phase angle of the reference surface velocity in air and in water with respect to the input electrical driving current are printed for each band in meters per second and degrees. Table A2 gives a sample of this information for the CTN ring at 9198 Hz. All of the numbers in the program output are printed with seven significant figures but for the tabulation are

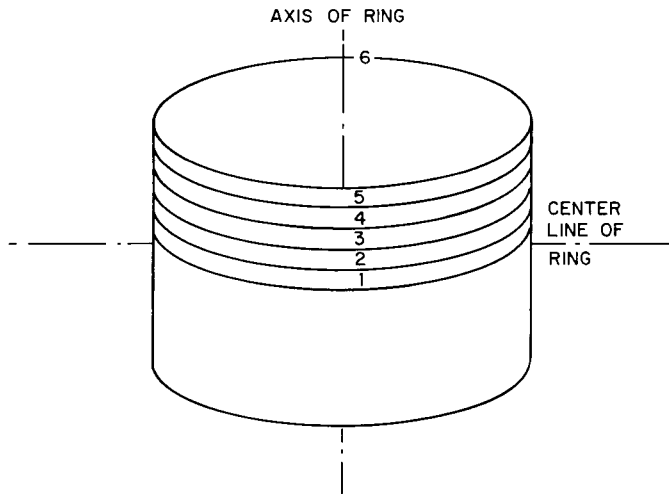


Fig. A1 — Ring reference surface. Band 6 has no height or thickness, because it corresponds to the edge of a zero-thickness shell.

rounded off to four significant figures. In addition to calculating the reference surface velocities in water, the computer program calculates the actual surface velocities and surface pressures of the ring in water. The real part, imaginary part, absolute magnitude, and phase angle of the in-water surface pressure and velocity with respect to the input driving current are printed for 28 bands around the ring. For an unclamped ring in a free field 14 bands give unique results. Bands 1 through 5 are on the outside surface of the ring from the middle to the top, bands 6 through 9 are across the top edge of the ring, and bands 10 through 14 are on the inside surface of the ring from the top to the middle. The outside and inside surface bands are of equal width, and the edge bands, whose width is different from those of the surface bands, are of equal width. The band designations similarly continue from 15 to 28 down the inside surface, around the bottom edge and up the outside surface. For the CTN ring at 9198 Hz, the surface pressures and surface velocities in water at 15 milliamperes drive current are given in Table A3. Other parameters which are calculated and printed are listed in Table A4 with sample results for the CTN ring at 9198 Hz. All dimensions are assumed to be in MKS units. The calculated total electrical impedances in air (ZEA) and in water (ZEE) for the rings near their respective air and water resonance frequencies are listed in Tables A5a and A5b. The calculated electrical impedances are plotted with the corresponding measured impedances in Figs. A2a, A2b, A3a, and A3b.

The agreement between theory and experiment for the electrical input impedances near air resonance of the two rings was quite good, but this agreement does not indicate the real strength and accuracy of a sophisticated mathematical model. The description of the motion at radial resonance of a thin ring transducer whose height is small compared to its diameter is essentially a one-dimensional problem. To a first approximation all points in the ring execute uniform radial motion, a vibration mode which has been documented for a magnetostrictive ring transducer* and is analytically described in closed form.

*S. Butterworth and F.D. Smith, "The Equivalent Circuit of the Magnetostriction Oscillator," *Phys. Soc.* 43 (No. 2), 166 (1931).

Table A2
Simplified Sample Printout of Reference Surface Velocities
(m/s) for the CTN Ring at 9198 Hz

In-Air Velocity and Band Designation	Real Part $\times 10^{-3}$	Imag. Part $\times 10^{-4}$	Magnitude $\times 10^{-3}$	Angle (Degrees)
VEL (1)	8.261	1.285	8.262	0.89
VEL (2)	8.258	1.284	8.259	0.89
VEL (3)	8.252	1.283	8.253	0.89
VEL (4)	8.243	1.282	8.244	0.89
VEL (5)	8.230	1.280	8.231	0.89
VEL (6)	-0.487	-0.00758	0.487	-179.11

In-Water Velocity and Band Designation	Real Part $\times 10^{-5}$	Imag. Part $\times 10^{-4}$	Magnitude $\times 10^{-4}$	Angle (Degrees)
VEL (1)	4.049	-1.697	1.745	-76.58
VEL (2)	4.084	-1.695	1.744	-76.46
VEL (3)	4.149	-1.692	1.742	-76.23
VEL (4)	4.232	-1.688	1.740	-75.93
VEL (5)	4.324	-1.683	1.738	-75.59
VEL (6)	-0.239	0.100	0.103	103.43

Table A3
Simplified Sample Printout of Surface Pressures (N/m²) and Velocities (m/s)
of the CTN Rings at 9198 Hz

Band	Surface Pressures				Surface Velocities			
	Real $\times 10^2$	Imag. $\times 10$	Mag. $\times 10^2$	Angle	Real $\times 10^{-5}$	Imag. $\times 10^{-4}$	Mag. $\times 10^{-4}$	Angle
1	-1.373	2.109	1.390	171.3	-4.130	1.731	1.780	103.4
2	-1.325	2.100	1.341	171.0	-4.166	1.729	1.779	103.5
3	-1.223	2.087	1.241	170.3	-4.232	1.726	1.777	103.8
4	-1.056	2.075	1.076	168.9	-4.317	1.722	1.775	104.1
5	-0.788	2.088	0.815	165.2	-4.411	1.717	1.773	104.4
6	-0.141	1.925	0.239	126.2	-0.239	0.100	0.103	103.4
7	0.0579	1.592	0.169	70.03	-0.239	0.100	0.103	103.4
8	0.238	1.280	0.270	28.29	-0.239	0.100	0.103	103.4
9	0.426	0.997	0.438	13.17	-0.239	0.100	0.103	103.4
10	0.998	1.039	1.003	5.941	4.246	-1.653	1.706	-75.6
11	1.219	1.131	1.224	5.304	4.156	-1.658	1.709	-75.9
12	1.352	1.175	1.357	4.967	4.074	-1.662	1.711	-76.2
13	1.432	1.197	1.437	4.779	4.010	-1.665	1.712	-76.5
14	1.470	1.206	1.475	4.691	3.975	-1.666	1.713	-76.6

Departure from the simple one-dimensional model in air occurs when the height or thickness of the ring is not small compared to its mean diameter. For this condition other vibration modes are prominent and a more sophisticated analysis is required. The analysis of the cylinder described in Appendix C, for example, requires a multimode mathematical model, even near the cylinder's radial resonance frequency. In the cases in which the one-dimensional model is adequate, however, agreement of in-air data and theory

Table A4
Simplified Sample Printout of Output Parameters
of the CTN Ring at 9198 Hz

Output Parameter	Computer Language	Real Part	Imaginary Part
Electrical Power	PIN	3.551×10^{-4}	2.643×10^{-3}
Acoustical Power	PA	9.787×10^{-5}	3.439×10^{-4}
Power Conversion Efficiency	EFF	2.756×10^{-1}	—
Motional Impedance in Air	ZMOTA	7.287×10	-2.684
Electrical Impedance in Air	ZEA	7.416×10	1.057×10
Motional Impedance in Water	ZMOTW	2.902×10^{-1}	-1.512
Electrical Impedance in Water	ZEE	1.578	1.175×10
Blocked Electrical Impedance	ZB	1.288	1.326×10
Radiation Impedance	ZL	9.567×10^3	3.362×10^4
Transduction Coefficient	HL	1.643×10^4	-8.608×10^2
Magnetic Field in Coil	HR	5.226	—
Transmitting Response in Plane (dB)	TRP	4.820×10	—
Transmitting Response Axial (dB)	TRA	1.510×10	—
Permeability Due to Hysteresis	UH	2.387×10^{-5}	2.432×10^{-7}
Total Permeability	UHE	2.379×10^{-5}	-1.247×10^{-6}

should be good, because the data fed into the computer program were empirically derived from the experiment using the one-dimensional model.

The agreement between theory and experiment for the electrical input impedances in water of the two rings described in this report is a more demanding test of the mathematical model, because the acoustic radiation aspect of the model must be correct. The NRL computer program SHIP, which comprises the radiation part of NRL EIGSHIP, is designed for rapidly determining acoustic surface pressures, radiation impedances, and far-field radiation patterns for acoustic sources in the form of finite circular cylinders and free-flooded rings.* Axial symmetry of the radiation source is assumed in the use of SHIP, and the basic inputs to SHIP are frequency and the geometric parameters of the ring or cylinder. The normal-velocity distribution of the source must be correctly known and its geometry and motion must be axisymmetric for SHIP to deliver correct impedances, pressures, etc. The velocity distribution of the ring source in water is computed from the elastic part of NRL EIGSHIP, taking into account the net forces on each part of the ring due to the magnetostrictive driving field and the acoustic radiation field.

A number of additional assumptions and simplifications are made in the application of NRL EIGSHIP to the ring problem. The elastic and magnetostrictive parameters of the ring which are calculated from the one-dimensional model of its in-air motion are assumed to remain constant for the in-water excitation. The holder from which the ring is mounted in water and the toroidal windings around the ring core are assumed to be acoustically invisible and are not modeled in the analysis. Although the ring excitation in air is CW, it is pulsed in water to eliminate reflections at the ring and at the hydrophone

*P.H. Rogers, "SHIP (Simplified-Helmholtz-Integral Program): A Fast Computer Program for Calculating the Acoustic Radiation and Radiation Impedance for Free-Flooded-Ring and Finite-Circular-Cylinder Sources," NRL Report 7240, June 1972.

Table A5a
Calculated Total Electrical Impedances
of the CTN Ring

Frequency (Hz)	Impedance (ohms)			
	In Air: ZEA		In Water: ZEE	
	Real Part	Imag. Part	Real Part	Imag. Part
7,000	1.18	11.3	2.15	13.2
7,200	—	—	3.30	14.4
7,410	—	—	6.56	15.2
7,493	1.28	12.5	8.61	14.3
7,568	—	—	9.97	12.2
7,619	—	—	10.1	10.4
7,644	—	—	9.86	9.61
7,666	—	—	9.54	8.95
7,722	—	—	8.39	7.71
7,791	—	—	6.84	7.04
7,913	—	—	4.74	7.14
8,073	1.49	14.2	3.26	7.97
8,500	1.88	16.5	1.98	9.86
8,800	—	—	1.72	10.8
9,000	5.94	27.5	—	—
9,100	15.2	38.2	—	—
9,136	27.1	44.4	—	—
9,160	43.4	45.5	—	—
9,175	58.1	39.7	—	—
9,180	63.2	35.6	—	—
9,184	66.9	31.3	—	—
9,192	72.5	20.3	—	—
9,198	74.2	10.6	—	—
9,204	73.1	0.56	—	—
9,210	69.4	-8.60	—	—
9,215	64.8	-15.0	—	—
9,220	59.4	-19.9	—	—
9,229	49.1	-25.2	—	—
9,247	31.7	-26.6	—	—
9,268	19.3	-22.1	—	—
9,278	15.6	-19.6	—	—
9,352	4.84	-6.51	—	—
9,425	2.52	-0.40	—	—
9,500	—	—	1.53	12.4

Table A5b
Calculated Total Electrical Impedances
of the Nickel 200 Ring

Frequency (Hz)	Impedance (ohms)			
	In Air: ZEA		In Water: ZEE	
	Real Part	Imag. Part	Real Part	Imag. Part
8,000	3.01	19.9	3.84	21.2
8,500	3.31	21.5	5.21	23.6
9,000	3.69	23.2	8.73	26.2
9,144	—	—	10.7	26.7
9,379	—	—	15.1	25.5
9,465	—	—	16.6	24.0
9,518	4.20	25.2	17.4	22.8
9,598	—	—	18.0	20.5
9,648	—	—	18.0	19.0
9,709	—	—	17.5	17.3
9,741	—	—	17.0	16.4
9,832	—	—	15.3	14.6
9,999	4.92	27.7	11.7	13.3
10,500	6.34	31.7	—	—
10,558	—	—	5.55	16.5
11,037	—	—	4.29	19.3
11,100	13.9	45.1	—	—
11,300	31.4	60.5	—	—
11,365	50.4	67.5	—	—
11,387	61.3	68.4	—	—
11,412	77.6	65.9	—	—
11,420	83.8	63.7	—	—
11,423	86.2	62.6	—	—
11,436	96.8	56.0	—	—
11,450	107.9	44.8	—	—
11,462	115.4	31.4	3.98	21.3
11,474	119.4	15.0	—	—
11,490	116.8	-8.50	—	—
11,500	110.5	-22.0	—	—
11,526	84.0	-44.6	—	—
11,547	61.7	-49.4	—	—
11,571	42.1	-46.3	—	—
11,625	18.5	-31.5	—	—
11,718	6.11	-12.5	—	—
11,800	3.19	-3.06	—	—

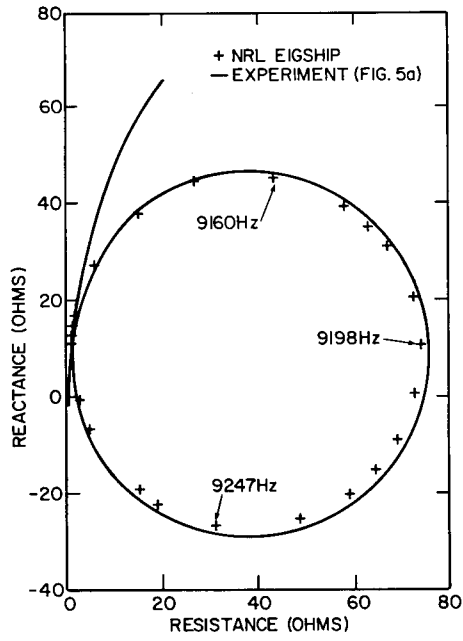


Fig. A2a — Electrical input impedance of the CTN ring near air resonance

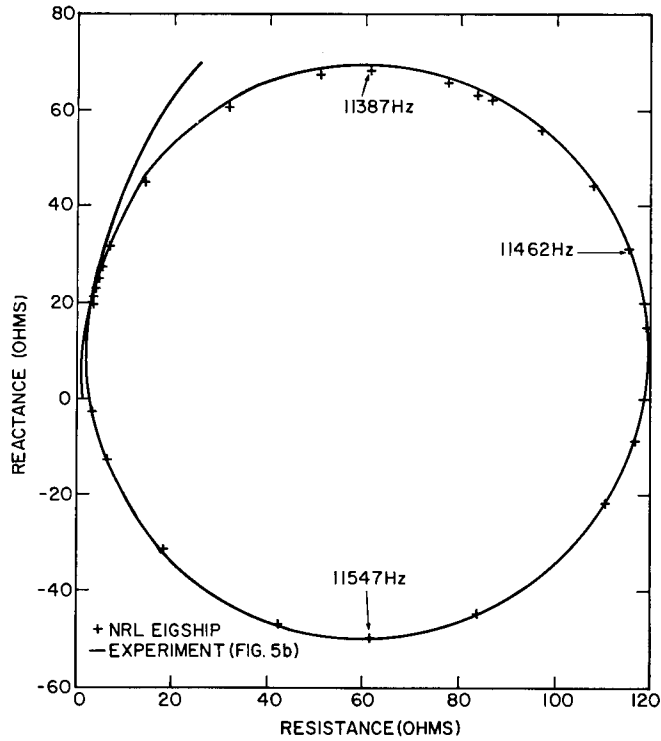


Fig. A2b — Electrical input impedance of the Nickel 200 ring near air resonance

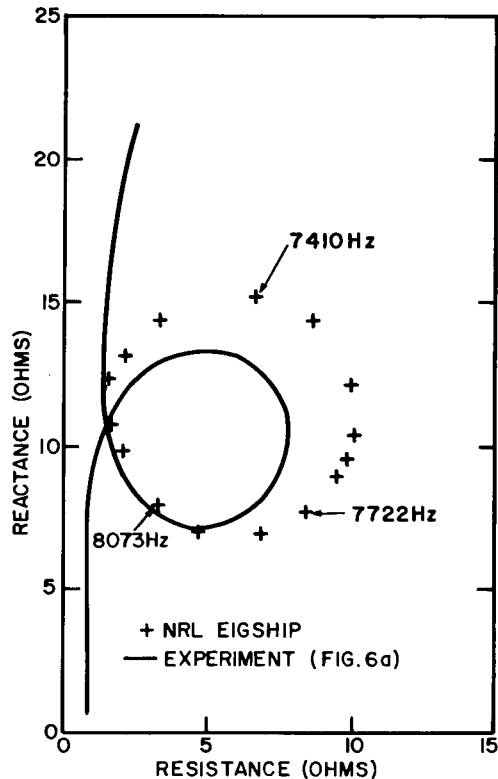


Fig. A3a — Electrical input impedance of the CTN ring in water

(used for transmitting responses) from the surfaces of the water and the NRL Acoustic Research Tank. All ring parameters are assumed to remain unchanged from CW to pulsed excitation. Finally, no trapped air is assumed to be in the proximity of the ring during the in-water measurements, because the presence of air bubbles alters the loading on the ring. The comparison between theory and experiment shown in Fig. A3 must be judged in view of these assumptions. Lack of agreement can be attributed to an experimental imperfection such as a nonuniformly fabricated or excited ring core or the presence of bubbles, to a theoretical error in the analysis or in the computer program, or to a failure of the theory to mathematically model aspects of the experiment which may be contributing significantly to the impedances such as the mounting structure or the toroidal windings.

Experiments were tried to determine the cause of the disagreement between theory and experiment (Fig. A3), but they yielded negative results. The number of toroidal windings was doubled, but the size of the theoretical in-water impedance loop exceeded that of the experimental loop by approximately the same percentages shown in Fig. A3. The ring mounts were altered and extraneous objects whose dimensions were comparable to elements of the ring mount were introduced into the field of the ring with no visible effect on the measured impedance loops. The calibration of the Scientific Atlanta Pulse Vector Immittance Meter was checked and found to be within manufacturer's specifications. The size of the in-water impedance loops varied according to the length of time

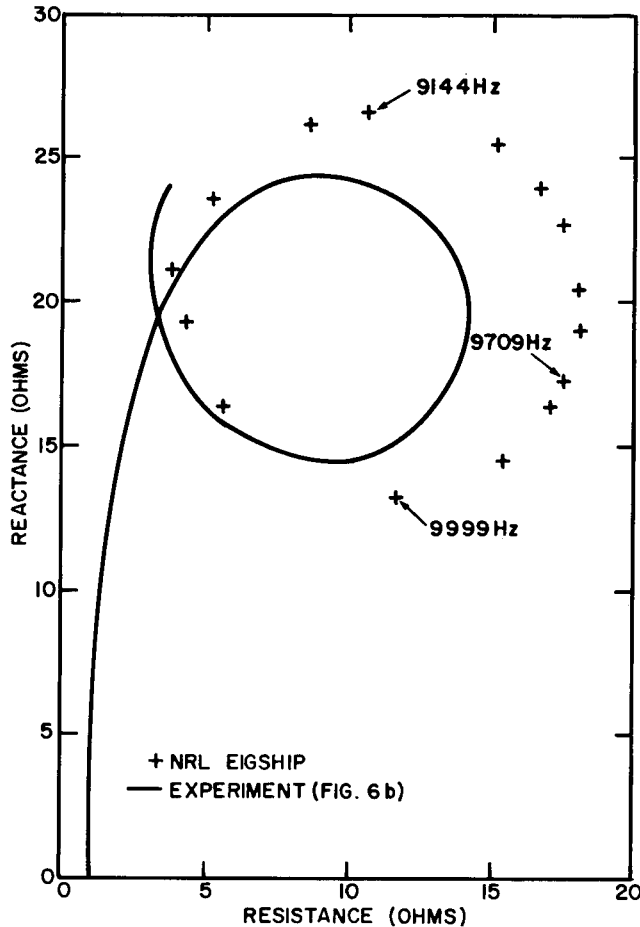


Fig. A3b — Electrical input impedance of the Nickel 200 ring in water

the ring was submerged, and for short-time submergence (dunking) a 100% variation in the size of the impedance loop was obtained. However following extended (overnight) submergence the size of the impedance loop was repeatable. This effect was attributed to trapped air bubbles which cling to the toroidal windings and which eventually dissipate during extended submergence. The impedance loop in water showed no significant change from pulsed to CW. No change resulted from replacing single-conductor stranded wire by single-conductor solid wire. In-air data taken immediately before and after extended submergence of the ring were repeatable, indicating that the ring core did not absorb water to the extent that its parameters measurably changed. Other similar Nickel 200 ring cores were excited in water, and the sizes of their impedance loops were essentially the same as the loop in Fig. 6b. The size of the impedance loop in water was independent of drive current magnitude from 15 to 150 milliamperes, thus implying linearity of the ring parameters over that dynamic range. This last test was done because the magnitude of the motion of the ring in air at radial resonance when driven with 15 milliamperes is approximately equal to the motion in water at radial resonance when driven with 150 milliamperes. Further attempts at resolving the disagreement between theory and experiment will be tried subject to the constraints of project funds and time.

Appendix B

A 1.9-INCH-HIGH RING

Rings whose dimensions were different than those discussed in the main body of the report were tested to provide a wider variety of data for comparison with theoretical ring-transducer models. However the only dimension that could conveniently be varied for either ring was the height of the CTN ring. The mandrel at the International Nickel Co. used to construct the CTN ring cores was of fixed diameter, but the CTN material was available in wider strip. The Nickel 200 ring cores were available in only one size. An intermediate-height CTN ring, discussed in this Appendix, and a CTN cylinder, discussed in Appendix C were constructed and tested.

A brief description by E. L. Huston of the International Nickel Co. was given of the construction technique of the ring core in a memo that accompanied the ring: "Forty-five feet of 0.008-inch nickel strip (S#06961) was slit to 1.9 inches wide, deburred, and cleaned with acetone. This strip was coiled with 0.010-inch expanded nickel-chrome screen and heat-treated to develop the *cube-on-face* texture and an insulating oxide coating. The scroll was consolidated with System 316 epoxy (Thermoset Plastics, Inc.) on a Teflon-lined wooden mandrel. The strip was pulled tight by hand and allowed to cure at room temperature overnight prior to extraction. Final dimensions and weights of the core were: mean diameter, 5.175 inches (0.1314 m); outside diameter, 5.445 inches (0.1383 m); inside diameter, 4.905 inches (0.1246 m); height, 1.941 inches (0.04930 m); and consolidated transducer weight, 1125 grams (1.125 kg).

The ring core was mounted exactly like the shorter height rings and wrapped with 144 turns of identical wire. Electrical-impedance and transmitting-response measurements similar to those previously described were taken on this ring, and the results are tabulated in Tables B1 through B3 and plotted in Figs. B1 through B4. All of the impedance measurements were made with a magnetic field intensity of 18 oersteds and an ac drive-current level which was kept constant at 15 milliamperes rms. The transmitting response was taken with an ac drive-current level of 100 milliamperes rms.

Table B1
Core Impedance of a 1.9-Inch CTN Ring In Air

Frequency (Hz)	Resistance (ohms)	Reactance (ohms)	Frequency (Hz)	Resistance (ohms)	Reactance (ohms)	Frequency (Hz)	Resistance (ohms)	Reactance (ohms)
500	1.3	1.5	13,000	4.2	39.3	32,000	22.0	99.6
1,000	1.4	3.1	14,000	4.6	42.7	33,000	23.3	102.4
1,500	1.4	4.9	15,000	5.2	46.2	34,000	24.6	105.3
2,000	1.4	6.7	16,000	5.9	49.5	35,000	26.1	108.4
2,500	1.4	8.3	17,000	6.6	52.8	36,000	27.6	111.4
3,000	1.5	10.1	18,000	7.4	56.0	37,000	29.2	114.2
3,500	1.6	12.0	19,000	8.1	59.2	38,000	30.8	117.2
4,000	1.6	13.8	20,000	8.9	62.2	39,000	32.3	120.1
4,500	1.7	15.5	21,000	9.8	65.4	40,000	34.0	122.9
5,000	1.8	17.2	22,000	10.6	68.5	41,000	35.7	125.9
5,500	1.8	19.2	23,000	11.6	71.6	42,000	37.5	128.9
6,000	2.1	21.1	24,000	12.6	74.8	43,000	39.4	131.8
6,500	2.2	23.1	25,000	13.6	77.7	44,000	41.3	134.5
7,000	2.4	25.2	26,000	14.6	80.8	45,000	43.1	137.3
7,500	2.7	27.9	27,000	15.6	83.9	46,000	45.0	140.2
8,000	3.2	31.4	28,000	16.7	86.9	47,000	47.1	143.2
10,000	2.2	23.5	29,000	17.8	90.0	48,000	49.1	146.0
11,000	2.8	31.0	30,000	19.3	93.1	49,000	51.3	149.0
12,000	3.4	35.6	31,000	20.6	96.0	50,000	53.5	151.8

JOEL A. SINSKY

Table B2
Impedance of a 1.9-Inch CTN Ring Near Air Resonance

Frequency (Hz)	Resistance (ohms)	Reactance (ohms)	Pulse-Vector-Immittance-Meter Scale (ohms)	Frequency (Hz)	Resistance (ohms)	Reactance (ohms)	Pulse-Vector-Immittance-Meter Scale (ohms)
9,000	20.6	71.5	100	9,153	138	-41	1,000
9,035	33.6	84.6	100	9,155	134	-45	1,000
9,065	49.2	93.6	100	9,157	129	-49	1,000
9,075	59.3	96.9	100	9,159	126	-51	1,000
9,080	66.2	98.8	100	9,161	122	-54	1,000
9,083	70.3	99.6	100	9,163	116	-57	1,000
9,086	74.2	99.9	100	9,165	112	-58	1,000
9,089	78.0	100.9	100	9,167	108	-60	1,000
9,091	81.8	100.8	100	9,169	104	-61	1,000
9,093	87.8	100.6	100	9,171	99	-63	1,000
9,095	91.1	99.8	100	9,171	98.6	-62.4	100
9,097	92.8	99.5	100	9,173	94.8	-62.6	100
9,099	99.3	97.9	100	9,175	90.4	-62.9	100
9,099	99	98	1,000	9,177	86.5	-63.2	100
9,101	102	97	1,000	9,179	85.0	-63.7	100
9,103	108	95	1,000	9,181	81.1	-64.1	100
9,105	113	93	1,000	9,183	76.8	-64.1	100
9,107	118	91	1,000	9,185	72.6	-63.6	100
9,109	124	88	1,000	9,187	70.0	-63.4	100
9,111	128	85	1,000	9,189	66.3	-62.9	100
9,113	132	82	1,000	9,191	63.4	-62.0	100
9,115	139	77	1,000	9,193	61.0	-61.6	100
9,117	142	73	1,000	9,195	57.9	-61.0	100
9,119	148	67	1,000	9,197	54.8	-59.7	100
9,121	151	62	1,000	9,199	53.0	-59.2	100
9,123	155	53	1,000	9,201	50.0	-57.0	100
9,125	158	48	1,000	9,204	46.8	-56.5	100
9,127	161	40	1,000	9,207	44.0	-55.2	100
9,129	162	32	1,000	9,210	41.9	-53.7	100
9,131	163	26	1,000	9,215	37.4	-51.3	100
9,133	164	19	1,000	9,226	29.8	-45.7	100
9,135	163	9	1,000	9,245	20.3	-36.0	100
9,137	163	5	1,000	9,260	15.5	-29.4	100
9,139	162	-1	1,000	9,280	11.2	-22.1	100
9,141	158	-11	1,000	9,345	5.1	-6.4	100
9,143	157	-15	1,000	9,381	3.7	-0.7	100
9,145	155	-20	1,000	9,403	3.2	1.6	100
9,147	152	-27	1,000	9,500	2.2	9.6	100
9,149	147	-33	1,000	9,800	2.0	19.9	100
9,151	142	-36	1,000	10,000	2.2	23.3	100

Table B3
Impedance of a 1.9-Inch CTN Ring In Water

Frequency (Hz)	Resistance (ohms)	Reactance (ohms)	Frequency (Hz)	Resistance (ohms)	Reactance (ohms)	Frequency (Hz)	Resistance (ohms)	Reactance (ohms)
500	1.4	1.4	7,000	3.6	20.8	18,000	7.6	52.8
1,000	1.3	3.1	7,500	3.7	22.4	19,000	8.0	55.7
1,500	1.0	4.8	8,000	3.8	23.8	20,000	8.6	58.7
2,000	1.0	6.3	8,500	3.9	25.0	21,000	9.3	61.5
2,500	1.3	8.0	9,000	4.0	26.4	22,000	10.1	64.4
3,000	1.4	9.5	10,000	4.0	29.2	23,000	11.0	67.2
3,500	1.5	11.3	11,000	4.0	32.0	24,000	11.8	70.2
4,000	1.6	13.1	12,000	4.1	35.2	25,000	12.7	73.0
4,500	1.8	14.9	13,000	4.6	38.0	26,000	13.7	75.9
5,000	2.6	17.0	14,000	4.8	41.3	27,000	14.6	78.6
5,500	4.1	17.9	15,000	5.4	44.6	28,000	15.8	81.1
6,000	4.0	18.2	16,000	6.3	47.6	29,000	16.6	83.9
6,500	3.7	19.5	17,000	7.1	50.2	30,000	17.8	86.7

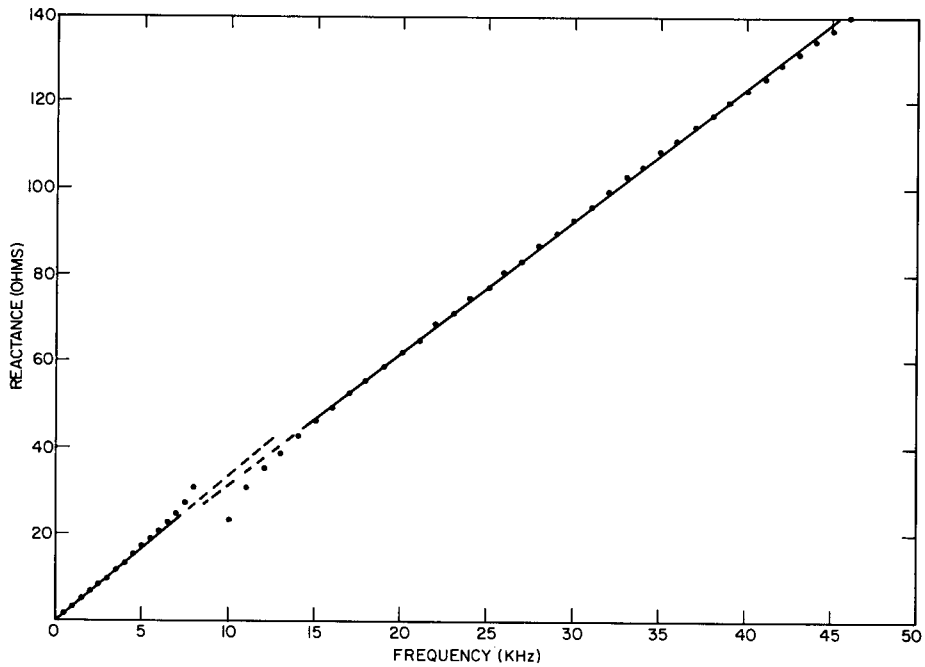


Fig. B1 — Core reactance of the 1.9 inch CTN ring

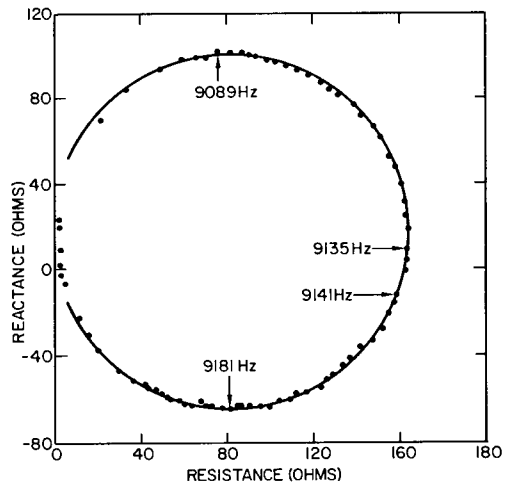


Fig. B2 — Electrical input impedance of the 1.9-inch CTN ring near air resonance

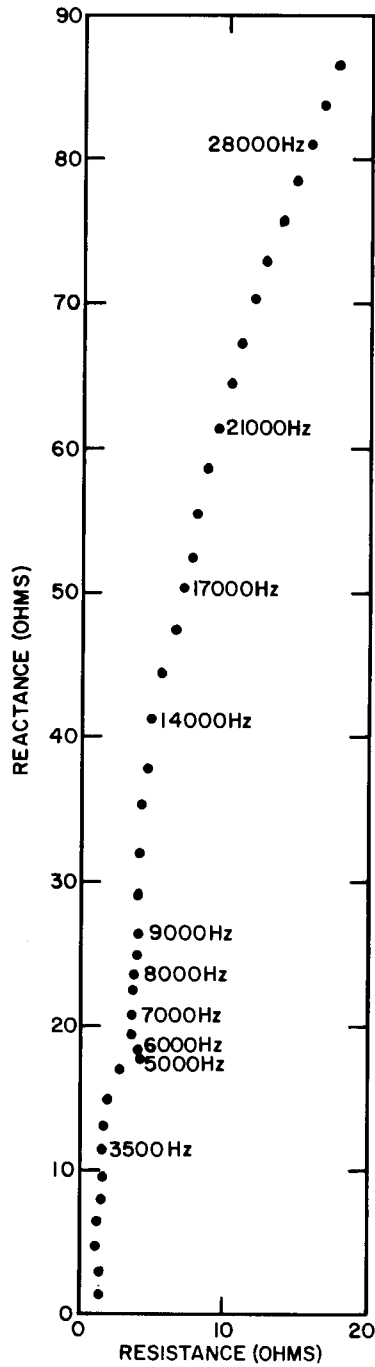


Fig. B3 — Electrical input impedance of the 1.9-inch CTN ring in water

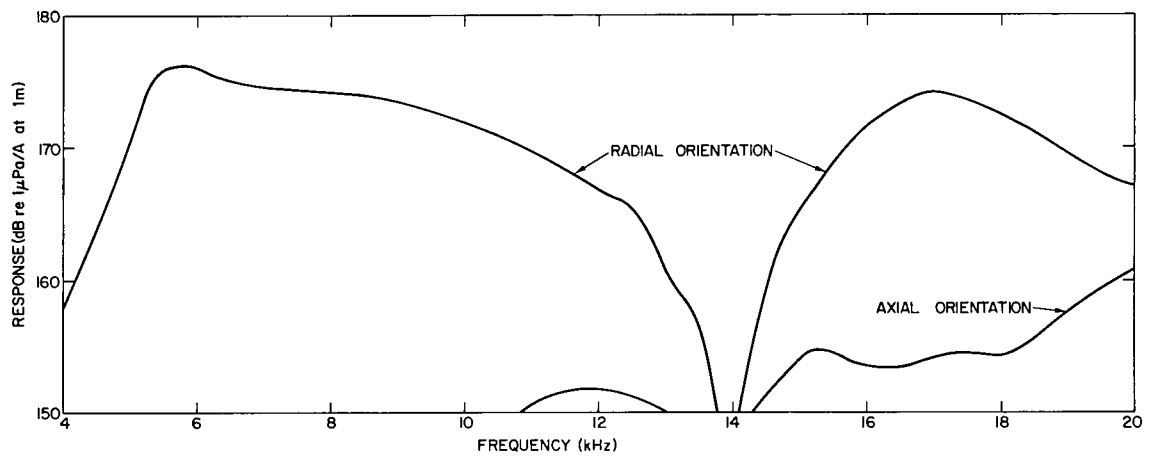


Fig. B4 — Far-field transmitting-current response of the 1.9-inch CTN ring

Appendix C

A 3.6-INCH-HIGH RING (CYLINDER)

A second significant variation in ring dimensions was tested, and in this case the height was sufficiently great to label the tested object a cylinder rather than a ring. The cylinder exhibits a barrelike mode of oscillation at frequencies close in value to the frequency of fundamental radial resonance. Consequently the mathematical model of the "ring" is severely tested insofar as it must predict and analyze more than one mode of oscillation. Once again the core material was CTN and the cylinder was fabricated by E. L. Huston of the International Nickel Corp., Suffern, New York.

Core construction was identical with that described for the previous rings. The final dimensions and weight of the core were: mean diameter, 5.185 inches (0.1317 m); outside diameter, 5.450 inches (0.1384 m); inside diameter, 4.919 inches (0.1249 m); height = 3.56 inches (0.09042 m); and consolidated transducer weight, 1921.8 gram (1.922 kg). The cylinder core was mounted exactly like the other rings and wrapped with 144 turns of the same gauge wire.

Electrical impedance and transmitting response measurements were taken on the cylinder, and the results are tabulated in Tables C1 through C3 and plotted in Figs. C1 through C4.

Table C1
Core Impedance of the CTN Cylinder in Air

Frequency (Hz)	Resistance (ohms)	Reactance (ohms)	Pulse-Vector-Immittance-Meter Scale (ohms)	Frequency (Hz)	Resistance (ohms)	Reactance (ohms)	Pulse-Vector-Immittance-Meter Scale (ohms)
500	1.2	2.8	100	26,000	26	130	1,000
1,000	1.1	5.5	100	27,000	28	135	1,000
2,000	1.4	11.3	100	28,000	30	140	1,000
3,000	1.6	17.3	100	29,000	35	147	1,000
4,000	1.7	23.1	100	30,000	37	152	1,000
5,000	2.3	29.3	100	31,000	40	156	1,000
6,000	3.0	36.0	100	32,000	42	161	1,000
7,000	3.8	43.5	100	33,000	45	166	1,000
8,000	6.2	57.0	100	34,000	48	171	1,000
10,000	2.7	37.0	100	35,000	51	176	1,000
11,000	4.1	49.1	100	36,000	54	181	1,000
12,000	5.3	56.6	100	37,000	57	185	1,000
13,000	6.5	62.9	100	38,000	60	189	1,000
14,000	7.7	68.7	100	39,000	64	194	1,000
15,000	9.0	74.4	100	40,000	67	199	1,000
16,000	10.4	79.9	100	41,000	71	204	1,000
17,000	11.9	85.5	100	42,000	75	209	1,000
18,000	13.4	90.7	100	43,000	79	213	1,000
19,000	14.9	95.6	100	44,000	83	219	1,000
20,000	16.5	101.3	100	45,000	87	223	1,000
21,000	17	105	1,000	46,000	90	228	1,000
22,000	17	110	1,000	47,000	95	232	1,000
23,000	20	116	1,000	48,000	100	236	1,000
24,000	22	120	1,000	49,000	104	240	1,000
25,000	24	126	1,000	50,000	109	245	1,000

Table C2
Impedance of the CTN Cylinder Near Air Resonance

Frequency (Hz)	Resistance (ohms)	Reactance (ohms)	Frequency (Hz)	Resistance (ohms)	Reactance (ohms)
8,000	6	57	8,957	246	-80
8,400	9	71	8,960	236	-89
8,600	15	88	8,964	220	-98
8,800	54	146	8,967	210	-112
8,850	107	176	8,970	203	-117
8,855	119	177	8,974	191	-122
8,860	129	181	8,977	177	-124
8,864	139	181	8,980	171	-128
8,868	147	180	8,983	162	-129
8,872	161	180	8,986	149	-131
8,876	168	179	8,989	141	-131
8,880	179	171	8,992	129	-133
8,885	189	164	8,995	121	-132
8,890	205	156	8,998	117	-129
8,895	213	149	9,001	107	-129
8,900	246	133	9,004	100	-128
8,904	253	128	9,007	93	-125
8,908	257	113	9,010	87	-123
8,911	267	98	9,015	77	-119
8,914	270	88	9,021	63	-112
8,917	273	77	9,027	57	-107
8,921	278	64	9,048	34	-84
8,924	281	51	9,071	22	-64
8,928	282	24	9,102	13	-44
8,931	281	18	9,200	3	-7
8,934	280	7	9,307	2	8
8,937	278	-3	9,408	2	17
8,941	273	-24	9,500	4	22
8,946	263	-44	9,800	3	33
8,950	256	-57	10,000	3	37
8,954	251	-72			

Table C3
Impedance of the CTN Cylinder In Water

Frequency (Hz)	Resistance (ohms)	Reactance (ohms)	Frequency (Hz)	Resistance (ohms)	Reactance (ohms)	Frequency (Hz)	Resistance (ohms)	Reactance (ohms)
500	1.1	2.4	4,500	3.2	22.1	8,265	7.2	39.0
1,000	1.1	4.9	5,000	2.4	24.8	8,288	7.2	39.0
1,500	1.1	7.6	5,500	2.4	27.6	8,328	7.0	39.3
2,000	1.2	10.2	6,000	2.6	30.4	8,360	7.0	39.5
2,500	1.3	13.1	6,500	2.9	32.9	8,401	6.9	39.7
3,000	1.5	16.1	7,000	3.3	35.3	8,500	6.9	39.9
3,500	1.8	19.6	7,500	4.0	38.3	9,000	6.8	41.5
3,700	2.6	21.4	7,700	4.6	40.0	9,500	6.6	43.1
3,800	3.3	22.2	7,800	5.3	41.4	10,000	6.3	45.1
3,828	3.8	22.2	7,835	5.9	41.9	10,500	5.9	47.5
3,851	4.0	22.4	7,851	6.3	42.2	11,000	5.8	49.7
3,870	4.2	22.4	7,870	6.8	42.4	12,000	6.0	54.9
3,886	4.4	22.4	7,888	7.5	42.5	13,000	6.6	60.0
3,900	4.5	22.3	7,901	7.9	42.4	14,000	7.3	65.2
3,920	4.8	22.2	7,912	8.3	42.3	15,000	8.8	70.4
3,936	4.9	22.2	7,925	8.8	42.1	16,000	10.5	74.6
3,952	5.0	22.1	7,938	9.1	42.0	17,000	11.3	77.8
3,965	5.1	22.0	7,950	9.3	41.6	18,000	11.7	82.0
3,979	5.2	21.9	7,962	9.6	41.3	19,000	12.3	86.8
3,993	5.2	21.8	7,972	9.8	41.0	20,000	13.3	91.2
4,012	5.3	21.7	7,983	9.9	40.6	22,000	15.8	100.8
4,026	5.3	21.6	7,991	9.8	40.3	Change from 100-ohm PVIM Scale to 1000-ohm Scale		
4,044	5.3	21.4	8,000	9.9	40.2			
4,068	5.3	21.3	8,010	9.8	39.8	22,000	15	99
4,090	5.2	21.1	8,027	9.7	39.4	24,000	17	108
4,109	5.2	20.9	8,042	9.5	39.0	26,000	20	117
4,126	5.1	20.8	8,055	9.4	38.8	28,000	24	125
4,144	5.0	20.8	8,069	9.2	38.8	30,000	27	132
4,164	4.9	20.8	8,082	8.9	38.5	32,000	31	141
4,184	4.8	20.7	8,097	8.7	38.4	34,000	35	150
4,203	4.6	20.7	8,108	8.4	38.4	36,000	37	157
4,224	4.4	20.8	8,121	8.2	38.4	38,000	41	164
4,243	4.3	20.8	8,136	8.0	38.4	40,000	45	171
4,263	4.2	20.9	8,150	7.9	38.5	42,000	48	177
4,283	4.0	21.0	8,166	7.8	38.5	44,000	52	184
4,300	3.9	21.2	8,180	7.7	38.7	46,000	55	189
4,329	3.8	21.3	8,197	7.5	38.8	48,000	58	195
4,364	3.6	21.4	8,218	7.3	38.8	50,000	63	199
4,400	3.4	21.5	8,240	7.3	39.0			

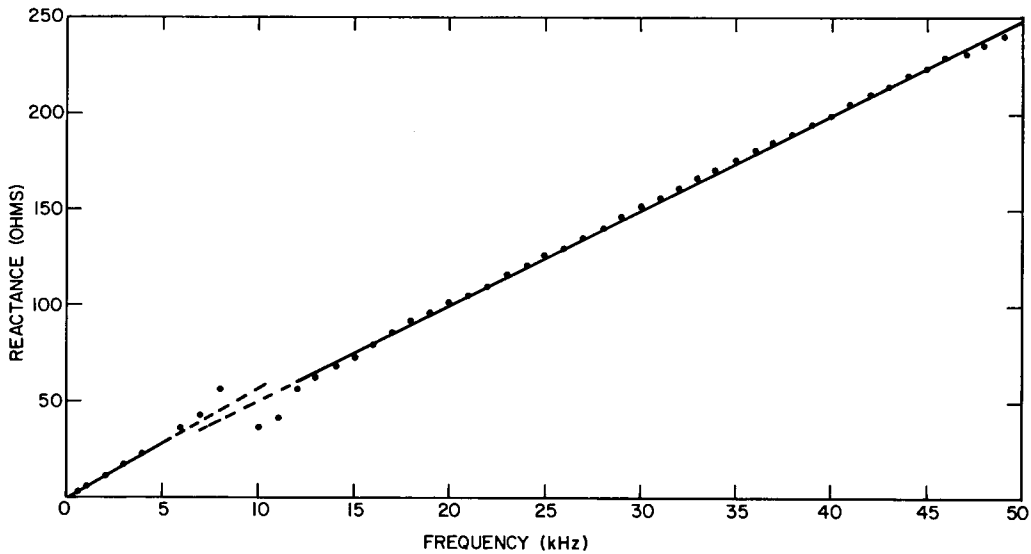


Fig. C1 — Core reactance of the CTN cylinder

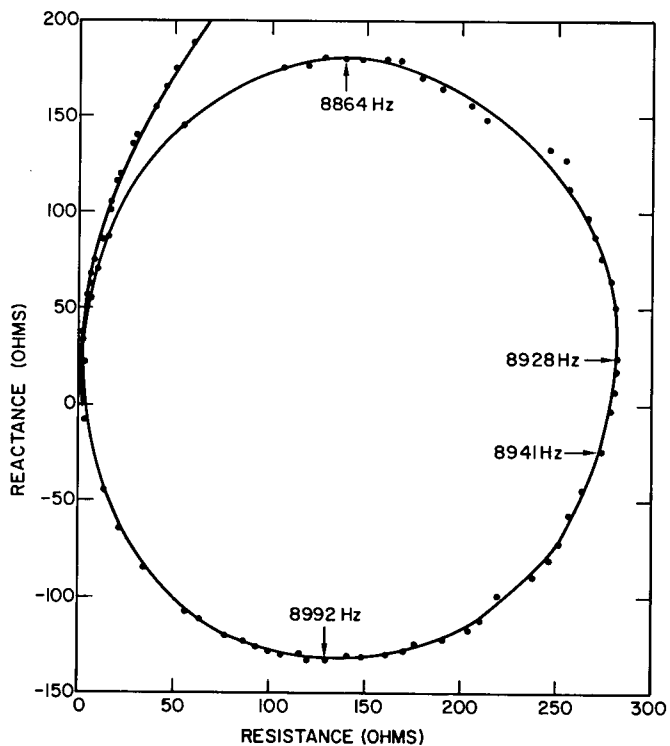


Fig. C2 — Electrical input impedance of the CTN cylinder near air resonance

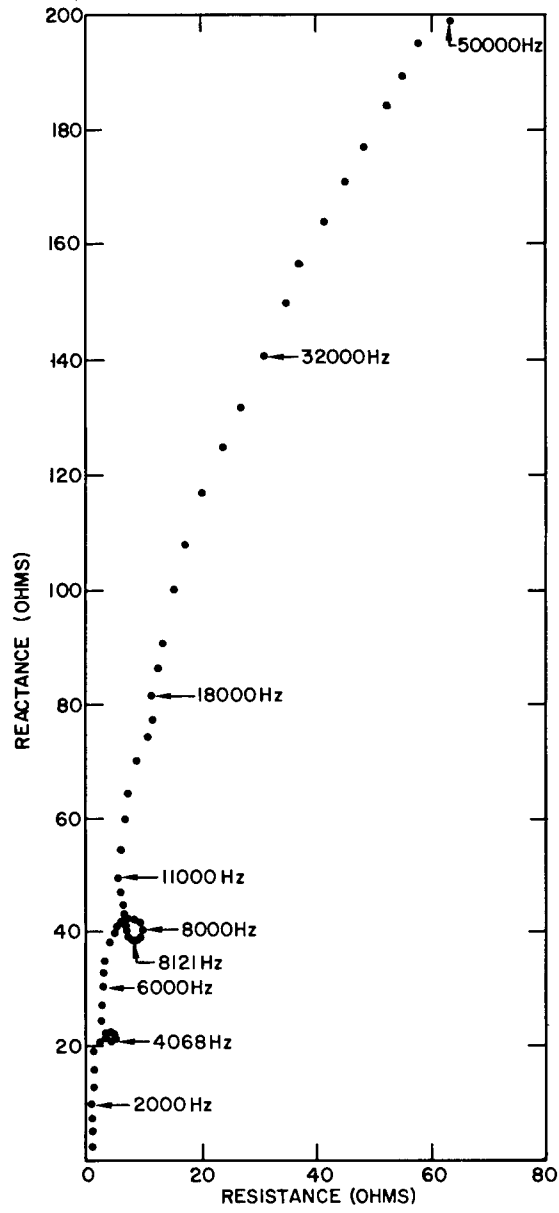


Fig. C3 — Electrical input impedance of the CTN cylinder in water

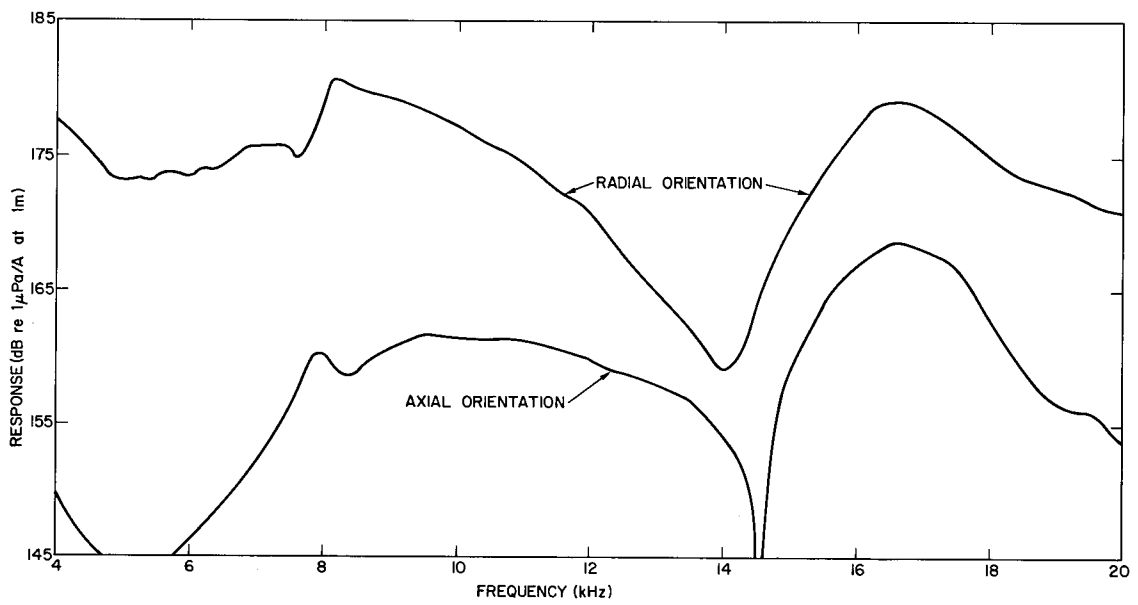


Fig. C4 — Far-field transmitting-current response of the CTN cylinder

